AD-A141 248 A THREE DIMENSIONAL FINITE ELEMENT ANALYSIS OF DELAMINATION GROWTH IN COM. (U) DREXEL UNIV PHILADELPHIA PA A S WANG ET AL. SEP 83 NADC-84017-60 1/1

UNCLASSIFIED N62269-82-C-0250 F/G 12/1 NL

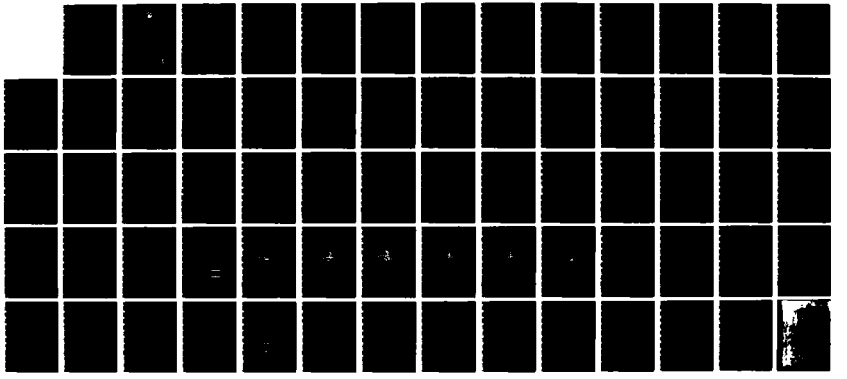

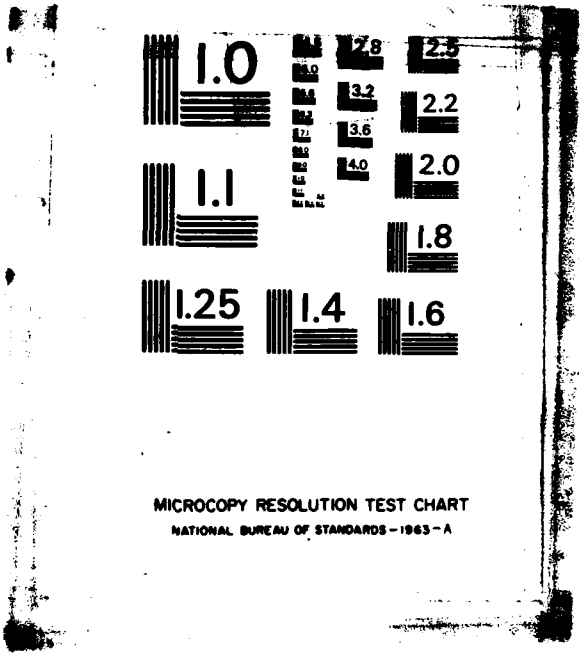
1.0
1.1
1.25
1.4
1.6
1.8
2.0
2.2
2.5
2.8
3.2
3.6
4.0
MICROCOPY RESOLUTION TEST CHART
NATIONAL BUREAU OF STANDARDS-1963-A

REPORT NO. NADC-84017-60

A THREE DIMENSIONAL FINITE ELEMENT ANALYSIS OF DELAMINATION GROWTH IN COMPOSITE LAMINATES

I. The Energy Methods And Case-Study Problems

A.S.D. Wang, M. Slomiana and R. Bucinell

Drexel University

Philadelphia, PA 19104

September, 1983

FINAL CONTRACT REPORT

CONTRACT NO. N-62269-82-C-0250

Approved for Public Release: Distribution Unlimited

Prepared for

Aircraft and Crew Systems Technology Directorate

NAVAL AIR DEVELOPMENT CENTER

Warminster, PA 18974

NOTICES

REPORT NUMBERING SYSTEM – The numbering of technical project reports issued by the Naval Air Development Center is arranged for specific identification purposes. Each number consists of the Center acronym, the calendar year in which the number was assigned, the sequence number of the report within the specific calendar year, and the official 2-digit correspondence code of the Command Office or the Functional Directorate responsible for the report. For example: Report No. NADC-78015-20 indicates the fifteenth Center report for the year 1978, and prepared by the Systems Directorate. The numerical codes are as follows:

CODE	OFFICE OR DIRECTORATE
00	Commander, Naval Air Development Center
01	Technical Director, Naval Air Development Center
02	Comptroller
10	Directorate Command Projects
20	Systems Directorate
30	Sensors & Avionics Technology Directorate
40	Communication & Navigation Technology Directorate
50	Software Computer Directorate
60	Aircraft & Crew Systems Technology Directorate
70	Planning Assessment Resources
80	Engineering Support Group

PRODUCT ENDORSEMENT – The discussion or instructions concerning commercial products herein do not constitute an endorsement by the Government nor do they convey or imply the license or right to use such products.

SECURITY CLASSIFICATION OF THIS PAGE (When Data Entered)

REPORT DOCUMENTATION PAGE

READ INSTRUCTIONS BEFORE COMPLETING FORM

1. REPORT NUMBER: NADC-84017-60	2. GOVT ACCESSION NO.: AD-A141248
3. RECIPIENT'S CATALOG NUMBER:	
4. TITLE (and Subtitle): A THREE DIMENSIONAL FINITE ELEMENT ANALYSIS OF DELAMINATION GROWTH IN COMPOSITE LAMINATES. Part I. The energy Method and Case Study Problems.	5. TYPE OF REPORT & PERIOD COVERED: Final Technical Report 1 Apr. 82 to 30 Sep. 83
	6. PERFORMING ORG. REPORT NUMBER:
7. AUTHOR(s): A. S. D. Wang, M. Slomiana and R. Bucinell	8. CONTRACT OR GRANT NUMBER(s): N- 62269-82-C-0250
9. PERFORMING ORGANIZATION NAME AND ADDRESS: Drexel University, Philadelphia, PA. 19104	10. PROGRAM ELEMENT, PROJECT, TASK AREA & WORK UNIT NUMBERS:
11. CONTROLLING OFFICE NAME AND ADDRESS: Aircraft and Crew Systems Technology Directorate Naval Air Development Center, Warminster, PA.	12. REPORT DATE: November, 1983
	13. NUMBER OF PAGES: 58
14. MONITORING AGENCY NAME & ADDRESS (if different from Controlling Office)	15. SECURITY CLASS. (of this report): UNCLASSIFIED
	15a. DECLASSIFICATION/DOWNGRADING SCHEDULE:

16. DISTRIBUTION STATEMENT (of this Report)

DISTRIBUTION STATEMENT A
Approved for public release; Distribution Unlimited

17. DISTRIBUTION STATEMENT (of the abstract entered in Block 20, if different from Report)

Approved for Public Release: Distribution Unlimited.

18. SUPPLEMENTARY NOTES

19. KEY WORDS (Continue on reverse side if necessary and identify by block number)
Delamination Growth, Fracture, Fatigue, Analytical Model, Energy Release Rate, Effective Flaw Concept, Two-Dimensional and Three-Dimensional Finite Element Simulations, Experimental Case Studies.

20. ABSTRACT (Continue on reverse side if necessary and identify by block number)

This report presents in detail the application of an energy method to describe a class of delamination growth problems found in polymer-based composite laminates. The energy method is derived from the general concept of the classical fracture mechanics. When used judiciously and with proper interpretation of the physical factors pertinent to the crack growth process at the lamina(ply) level, the method provides an anlytical simulation for the delamination process in laminates subjected to monotonic loading and/or cyclic loading, both in

DD FORM JAN 73 1473 EDITION OF 1 NOV 65 IS OBSOLETE
S/N 0102-LF-014-6601

UNCLASSIFIED
SECURITY CLASSIFICATION OF THIS PAGE

tension and in compression.

Case studies involving one-dimensional delamination growth(e.g. uniform free edge delamination) and two-dimensional delamination growth(contour delamination) have been performed along with laboratory tests using laminates made of AS-3501-06 graphite-epoxy system. Excellent correlation between experimental and predicted results has been achieved.

FOREWORD

This is the Final Technical Report, Part I, of a research program sponsored by the Aircraft and Crew Systems Technology Directorate, Naval Air Development Center, Warminster, Pennsylvania, 18974, under contract No. N-62269-82-C-0250. The NADC monitor was Mr. Lee W. Gause. Dr. A. S. D. Wang was the principal investigator; and he was assisted by Miss M. Slomiana and Mr. Ronald Bucinell, Drexel graduate students.

The primary objective of this research was to develop a computer routine which can be used to calculate the stress field of a laminate containing a propagating delamination crack. By incorporating a virtual crack opening procedure in the routine, the crack-front strain-energy release rate can be calculated as the delamination crack is incrementally propagated. Since a general delamination crack may have a contoured front, this routine is capable of adjusting to new boundary configurations and, at the same time, yielding an accurate three-dimensional stress field solution.

The timely development of the present routine represents a major step toward analytical treatment of delamination mechanisms, perhaps the most damaging failure mode in structural composite laminates.

In Part I, an overview of the energy release rate method is presented, as it is applied to describe delamination growth in laminates subjected to both static and fatigue loads. One-dimensional growth (free-edge delamination) as well as two-dimensional growth (countoured delamination) problems are studied. All results are correlated with past and/or present experimental data.

Part II presents details of the computer code used to perform these calculations. It is contained in the report NADC-84018-60.

INTRODUCTION

The delamination problem is one of the most important problems affecting the use of structural composite laminates. It is often encountered as the most damaging laminate failure mode. The mechanisms of delamination are extremely complex rendering a satisfactory analytical treatment practically untractable.

As far back as in the late 1960's, laboratory coupon tests had established that the tensile strength of a laminate depends on the laminate stacking sequence [1]. The stacking sequence could determine whether or not a free edge delamination would occur under the applied load. If a free edge delamination occured, it would rapidly propagate under increasing load, causing premature failure. This unique phenomenon can be present not only in laminates under tensile loads [2], but also in laminates under compressive loads [3], so long as the laminate stacking sequence is such that free edge delamination is induced by the applied load.

A relatively slower delamination growth can also be induced by cyclic loads, be it tensile and/or compressive [3]. Onset of delamination can occur at cyclically applied stress levels much below the threshold stress determined by static load. Generally, delamination growth considerably shortens the laminate's fatigue life.

Regardless of the nature of loading, edge delamination has been thought to be driven by the interlaminar stresses which exist near the laminate edge boundaries. Early analytical efforts have concentrated, therefore, on the determination of the free edge interlaminar stresses. These are highly concentrated near the intersections of the free edge and the lamina interfaces [4-6]. In fact, these intersection points are singular points [7], where the stress field is unbounded. Because of mathematical difficulties, rigorous

free edge stress analyses have been limited to the special problem of a long, uniform width and symmetrically stacked laminate subjected to uniaxial tension.

Nevertheless, these analyses have helped to unveil the complicated nature of the delamination mechanisms. In particular, knowledge of the interlaminar stresses, their signs and magnitudes, may determine whether or not a free edge delamination will occur.

Laboratory experiments have shown that the growth behavior of free edge delamination depends profoundly on the absolute thickness of the material layers of the laminate [8, 9]. For example, the onset of delamination and the subsequent growth behavior under tensile loading was significantly different between the $[\pm 45/0/90]_s$ and $[\pm 45_2/0_2/90_2]_s$ laminates, even though the calculated interlaminar stresses are identical both in sign and in magnitude [8].

Other complexities have been observed. The most perplexing are the phenomena of failure modes interactions. For instance, consider the $[\pm 45/0/90]_s$ laminate under uniaxial tension. In some tests, free edge delamination occured first, its growth inducing multiple transverse cracks in the 90-layer. Conversely, 90-layer transverse cracks occured first in other tests which then precipitate localized delaminations [9]. The growth of the latter is generally multi-directional, resulting in a contoured delamination front.

All these difficulties have complicated the development of a satisfactory analytical model. Even with a considerable experimental base emcompassing the various facets of delamination, no rational methodology which generally describes the onset and the growth of delamination had been devised.

In a series of recent papers [10 -14], Wang, Crossman, et. al successfully applied an energy method to model the onset and growth behavior of a class of simple matrix cracking problems. The type of cracks considered included the

afore-mentioned 90-layer transverse cracks and free edge delamination induced by statically applied tensile and compressive loads. Their model proved to be generally applicable when these two types of cracks occurred individually in a given laminate.

This paper extends the application of the energy method to fatigue load induced delamination growth, and the more complex contour delamination growth caused by two interacting flaws. Correlations between the analytical and the experimental results are also presented.

THE ENERGY RELEASE RATE METHOD

The energy method is based on the fundamental concept of classical fracture mechanics. Essentially, it involves nothing more than a judicious use of the crack growth criterion:

$$G(\sigma,a) = G_c \tag{1}$$

Equation (1) is the well known Griffith criterion for a brittle crack propagating in a self-similar manner inside a homogeneous solid [15]. It actually describes the energy balance at incipient propagation for a crack having a length "a" and under the applied load σ. But unlike in the classical text-book problems where the crack geometry(including the crack length a) and the material fracture toughness G_c are well defined apriori, these quantities are either generally unknown or difficult to determine for the types of cracks found in fibrous composites. In addition, mathematical computation of the function $G(\sigma,a)$ for a crack propagating in multi-layered anisotropic media could also become intractable.

In the Wang-Crossman approach, these limitations were largely overcome through the use of the following fundamental concepts as well as recent developments: (a) the fundamental postulate of the "effective" material flaw distribution which enables the definition of the initial crack length "a" as a random variable, (b) the expanded understanding of the quantity G_c as a local, mode-dependent and directionally variable material property, (c) the improvement of various damage detection methods which provided a visual description of the cracking process as a continous function of loading and/or time under load, and finally, (d) the development of suitable numerical procedures to compute $G(\sigma,a)$ for cracks propagating in multi-layered anisotropic solids. A brief discussion on some of the above aspects is given below.

The Concept of Effective Flaw Distribution.

In laminate stress analysis, the fundamental approach has been the so-called ply-elasticity theory [16]. The theory pertains primarily to laminates that are made of unidirectional plies stacked together, with each ply oriented in some designed direction. The individual plies, though consisting fibers and matrix phases, are assumed macroscopically homogeneous and having uniform material properties. This assumption enables characterization of the unidirectional plies by two sets of material constants. The first set consists of the ply deformation constants, while the second set is associated with the ply strength constants. For example, the stiffness matrix C_{ij} in the generalized Hooke's law and the strength constants F_{ij} and F_j in the quadratic failure criterion are among the most widely used ply properties [16]:

$$\sigma_i = C_{ij}e_j \qquad i,j = 1,6 \qquad (2a)$$

$$F_{ij}\sigma_i\sigma_j + F_j\sigma_j = 1 \qquad i,j = 1,6 \qquad (2b)$$

It is noted that the constants C_{ij}, F_{ij}, etc. are regarded as uniform property of the ply material, and they are usually determined experimentally from a specimen having finite volume. In particular, failure criterion such as expressed in Equation (2b) determines the first and only failure of the ply. As has been discussed earlier, multiple failures in a certain ply can occur at different stress levels when that ply is a part of a laminate. Hence, ply-strength cannot be regarded as a constant material property in this context.

The conceptual argument for multiple ply failures in laminates is that randomly distributed material flaws exist in the microstructure of the unidirectional plies and in the ply-to-ply interfaces. The true physical characteristics of the flaws are believed to be inherent to the basic ply material itself, and possibly also to the laminate fabrication process, post-process

handling, etc. Realistically, the true identity and the exact physical effect of the individual flaws cannot be determined within the context of the macro-theory of ply-elasticity. One useful alternative, however, is to introduce the concept of "effective" material flaws.

This concept theorizes that a characteristic distribution of "effective" flaws can be determined for a given representative volume of the basic ply material; each of the effective flaws has a definite size as well as location. Though hypothetical in nature, the effective flaws must be so characterized as to represent the aggregate effect of local microflaws and inperfections at the ply level. In this context, each effective flaw is further assumed to act like a small crack; and it's growth behavior may be describable by the Griffith criterion (1). Then, each of the effective flaws can individually become a sublaminate crack at some critical stress level; and they form collectively multiple sublaminate cracks in the course of loading.

Once the size, the location and the geometrical character of an effective flaw is defined in relation to the layering structure of the considered laminate, the flaw(crack) tip strain energy release rate $G(\sigma,a)$ can be calculated by some suitable computational method.

The Crack-Closure Procedure for $G(\sigma,a)$.

For a line crack in two-dimensional elastic solids, the stress field near the crack tip is singular in nature. The classical methods of solution have been to solve for the near-field stresses by means of a boundary-value problem in the theory of elasticity [17]. These stresses are generally obtained for three distinct modes of the crack action: the opening mode-I, the sliding mode-II and the anti-plane mode-III. For each mode there is an associated stress intensity factor, K_I, K_{II} and K_{III}. The latter are functions of the crack size "a" and the applied far-field stress σ [18]. The quantity $G(\sigma,a)$ can be

related directly to K_I, K_{II} and K_{III}. This procedure, however, can become mathematically intractable for problems that involve complex geometry, such as multiple cracks in layered composites.

Other solution techniques for $G(\sigma,a)$ are available, notably the well-known J-integral method [19,20] and the method of crack-closure by Irwin [21]. In particular, Irwin's method recognizes the equality between the elastic strain energy which is released during a virtual crack extension, and the work done in closing it again. The closing of the virtual crack extension, Δa, yields the solution for the required surface traction vector $\bar{\sigma}$ over Δa. And, the work done is

$$\Delta W(\sigma,a) = \frac{1}{2}\int^{\Delta a} (\bar{\sigma}\cdot\Delta\bar{u})\, da \qquad (3a)$$

where $\Delta\bar{u}$ is the relative crack surface displacement vector over Δa. Note that both $\bar{\sigma}$ and $\Delta\bar{u}$ depend on the crack size "a" and the applied far-field stress σ. Then, from the elastic equivalence the crack extension rate of strain energy release can be expressed by

$$G(\sigma,a) = \lim_{\Delta a\to 0} (\Delta W/\Delta a) \qquad (3b)$$

The advantage of expressing G in the form of (3a) and (3b) is that the vector product $(\bar{\sigma}\cdot\Delta\bar{u})$ yields a sum of three scalars which associate directly with the three modes of the cracking action. Hence, (3b) gives the sum of G_I, G_{II} and G_{III}. In addition, the integral in (3a) can easily be evaluated numerically by discretization of the solution field which contains the considered crack. For example, the traction vector $\bar{\sigma}$ and the crack extension displacement vector $\Delta\bar{u}$ may be approximated by the nodal forces and nodal displacements, respectively, in a finite element representation.

Rybicki and Kanninen [22] first suggested the finite element scheme for

simulating uniform free edge delamination in a laminate subjected to uniaxial extension. Wang and Crossman [10] extended the scheme in a generalized plane strain formulation allowing warping of the laminate's cross-section. Their finite element routine has been used successfully for transverse cracking and free edge delamination simulations [10-14].

The Physical Charateristics of G_c

The right-hand side of Equation (1) is a material property; the term G_c represents the material resistance against crack propagation, which must be measured experimentally. Generally speaking, the measured G_c depends on the local morphology of the fractured material surface. It is usually regarded as a constant in homogeneous, isotropic materials. For fibrous composites, however, the fractured surface morphology can differ greatly depending on the local matrix/fiber reinforcement geometry which can be both spatial and directional dependent. But, on the basis of ply-elasticity from which the fracture growth criterion (1) is applied, such local surface morphology cannot be concurrently distinguished. For this reason, laboratory measured G_c in matrix-dominate crack growth has been found to depend on the propagation direction and the local fiber and/or ply-interface orientation [23].

For example, Cullen [24] and William [25] considered two different cases of mode-I delamination growth in unidirectional laminates, see illustrations in Figure 1. The first case concerned the crack propagating in the fiber direction, while the second case concerned the crack propagating normal to the fiber direction. The actual fractured surface morphology of the two cases was found to exhibit a considerable amount of differences. And, as a result, the respective measured G_c also differed significantly. Form the view point of ply-elasticity, however, these two cases should not display any difference.

Another aspect of the measured G_c is related to mixed-mode cracks that

contain both opening and shearing modes. Apparently, the total strain energy dissipated in a mixed-mode crack extension is greater than in a purely mode-I crack extension. The increase in the measured G_c is generally attributed to crack-tip matrix yielding under shear deformation. In several recent experiments on graphite-epoxy composites, the total G_c for mixed-mode matrix cracks was found to increase with G_{II}/G_I ratio [26-28]. Consequently, if the growth criterion (1) is used for mixed-mode cracking, G_c is multiple-valued; see, e.g. the curve shown in Figure 2.

Although other alternate criteria for mixed-mode cracks have been used in various crack growth situations, which normally require more than one constant (e.g. G_{Ic}, G_{IIc}, G_{IIIc}, etc.), questions surrounding the existence of and the determination method for the constants have not been resolved for cracks propagating in composites. Apparently, the exact mechanisms in mixed-mode cracking must be examined carefully at the microscopic scale. Such a topic still remains an area of future research.

In view of the foregoing discussions, it is clear that the classical criterion as expressed in Equation (1) cannot be applied straight-forwardly for sublaminate crack growth problems in composite laminates. Judicious interpretations for each of the elements in the equation must be made in order to develop a viable analytical model for the cracking phenomenon as observed at the macroscopic scale.

As has been mentioned previously, the energy approach has been applied successfully to describe the formation process of multiple transverse cracks in laminates loaded monotonically or cyclically [29]. The same approach also proved applicable to model uniform free edge delamination growth when it is not interacting with other modes of cracking [30].

Some key features of the free edge delamination model will be presented

next, along with an extended model for fatigue load induced delamination growth. Both one-dimensional and two-dimensional growth problems will be analyzed and compared to experimental case study results.

ONE - DIMENSIONAL GROWTH PROBLEMS

Consider the laminate having a finite width and subjected to uniform axial tensile strain $\bar{e}_x$; see inset in Figure 3. Let the laminate stacking sequence be such that tensile interlaminar normal stress σ_z is induced near the laminate free edge region. Assume that an effective interlaminar flaw having a random size "a" exists along the edge as shown. When the free edge stress field reaches a certain critical state, the effective flaw will propagate and form a crack opening on the free edge. This event then constitutes the "onset" of free edge delamination, and the concurrent stress state is termed the threshold stress.

For clarity, let it be assumed that the particular interface in which delamination will occur is known apriori. Then, the flaw(crack) tip energy release rate $G(\bar{e}_x,a)$ for the assumed effective flaw "a" can be calculated by the finite element crack-closure procedure. For a given value of $\bar{e}_x$, G will vary with "a". A typical G-curve is shown in Figure 3. It is seen that G rises sharply from zero at $a = 0$, and reaches an asymptotic value G_m at $a \geq a_m$

It is of interest to note that although a stress singularity may exist at the free edge/ply interface intersection [7], a non-trivial G could be determined only when an effective flaw of size $a > 0$ is introduced near the ply interface.

As for the value of a_m, it is usually of the order of the ply thickness. Hence, the value of G_m can be affected by the ply-thickness parameter [14].

With linear elastic plies, it is often convenient to express G in explicit terms of the applied strain $\bar{e}_x$. For instance

$$G(\bar{e}_x,a) = C_e(a) \cdot t \cdot \bar{e}_x^2 \qquad (4)$$

where C_e is a function of the flaw size (a/t) only; and t is a chosen length parameter, usually taken as one ply thickness.

Similarly, if the laminate is subjected to a uniform temperature load, ΔT, and the thermally induced free edge stresses can also effect delamination, then the associated flaw tip energy release rate G is expressible as,

$$G(\Delta T, a) = C_T(a) \cdot t \cdot \Delta T^2 \qquad (5)$$

Where C_T is also a function of the flaw size (a/t) only, and whose functional shape is similar to that shown for C_e.

Normally, ΔT is determined experimentally to represent the temperature drop from the stress-free temperature($\leq$ laminate curing temperature) to the ambient service temperature.

The mechanical and the temperature load effects on the laminate stress field are linearly additive; and the total energy release rate for the combined loading case can be expressed as,

$$G(\bar{e}_x, \Delta T, a) = \left[\sqrt{C_e} \cdot \bar{e}_x + \sqrt{C_T} \cdot \Delta T\right]^2 \cdot t \qquad (6)$$

If the size of the edge flaw "a" is given, then the onset of it's propagation(also delamination) is defined when the applied laminate strain $\bar{e}_x$ is such that

$$G(\bar{e}_x, \Delta T, a) = G_c \qquad (7)$$

With "a" being random valued, however, Equation (7) can be plotted in the $\bar{e}_x$ versus "a" plane. Then, given a range of possible values for the edge flaw size, a corresponding range for the onset load(i.e. $\bar{e}_x$) can be determined from the plot as shown in Figure 4. In particular, if for all probabilities the size of the edge flaw is of the order of a_m or larger, then the predicted load range for onset of delamination is very narrow; in fact, it becomes practically a constant, see Figure 4. The latter represents the minimum possible load for onset of delamination.

Illustrative Example - Laminates Under Static Tension.

In order to illustrate the use of the energy model outline above, consider the laminate family $[\pm 25/90_n]_s$, n = 1,2 and 3. The laminates were made using AS-3501-06 graphite-epoxy system, and were tested at room temperature under static uniaxial tension (for details, see Ref. [30]). Free edge delamination growth was induced in all laminates during the course of loading. Figure 5 shows the experimental plot for delamination size versus applied laminate stress $\bar{\sigma}_x$. In each of the three types of laminates, three replicates were used; and an averaged onset load for delamination could be determined by extrapolation of the delamination growth curve.

Post-test examination of the specimens showed that delamination in the $[\pm 25/90]_s$ laminate was contained in the mid-plane, while delamination in the $[\pm 25/90_2]_s$ and the $[\pm 25/90_3]_s$ laminates was in the -25/90 interface. Actually, 90-layer transverse cracks in the latter two laminates were observed to precede free edge delamination. When delamination occurred, it was mostly localized near clusters of transverse cracks [30]. The latter is, of course, a case of "crack modes interaction", which will be treated later in this paper as a two-dimensional contour delamination growth problem.

Only in the $[\pm 25/90]_s$ laminate was onset of edge delamination not complicated by transverse cracks. The delamination grew uniformly along the length of the specimen. Hence, the fracture model for one-dimensional growth as outlined above could be applied. Using the base properties of the unidirectional ply (see Ref. [30] for values) in the energy release rate calculation, the coefficient functions appearing in Equation (6) were generated for an assumed delamination in the laminate mid-plane and in the -25/90 interface. These calculated functional curves are displayed in Figures 6 and 7, respectively.

It is noted that mid-plane delamination is of mode-I due to symmetry in

the lamination stacking sequence, while -25/90 interface delamination is of mixed-mode (I and III). In the present example, G_{III} is about 0.8 times of G_I.

From Figures 6 and 7, it is seen that the total energy release rate for mid-plane delamination is larger than that for -25/90 interface delamination. Furthermore, the material resistance G_c for mode-I growth is smaller than that for mixed-mode growth (see, e.g. Figure 2). Thus, the model would predict a mid-plane, mode-I delamination growth. Using the maximum values of C_e and C_T in Figures 6 and 7, the minimum onset load (in terms of far-field laminate strain $\bar{e}_x$) can be calculated from Equations (6) and (7); thus,

$$(\bar{e}_x)_{min} = 0.53\ \%$$

In computing above, $G_{Ic} = 175\ J/m^2$ (1.0 in-lb/in^2), t = 0.132 mm (0.005") and $\Delta T = 125^oC$ (225^oF) were used, see Ref. [30].

For the laminate considered, the axial modulus $\bar{E}_x$ = 64 Gpa (9.3 msi); then the calculated minimum onset far-field stress is,

$$(\bar{\sigma}_x)_{min} = 338\ \text{Mpa}\ (49.0\ \text{ksi}).$$

Extrapolating the experimental value for $(\bar{\sigma}_x)_{cr}$ from Figure 5 yields a range from 331 to 345 Mpa (48 to 50 ksi). The prediction falls in this range.

Illustrative Example - Laminates Under Static Compression.

To further assess the usefulness of the energy model, consider the following laminates which are geometrically similar: $[90_2/0_2/\pm45_2]_s$, $[0_2/90_2/\pm45_2]_s$ and $[(0/90)_2/(\pm45)_2]_s$. These laminates were also made using the AS-3501-06 graphite-epoxy system; but they were tested in room temperature under static compressive loading. In each test case, three replicate specimens were used.

The stacking sequence of all the three types of laminates was designed to yield a tensile interlaminar normal stress σ_z near the free edge under the

applied compressive load. And, indeed, edge delamination in the laminate mid-plane was induced in all test cases (detailed test data may be found in Ref. [3]. Figure 8 shows the delamination growth as plotted against the applied stress $\bar{\sigma}_x$ for each of the three types of laminates. The growth curves indicate that onset of edge delamination was followed by a rapid growth, which caused the final failure of the laminates. Note, in particular, that the onset load for delamination differed appreciably among the three types of laminates, though they are in many ways similar to one another.

A free edge stress analysis was performed in order to discern any major differences which may be present in their free edge stress distributions. Figures 9, 10 and 11 show the through-thickness σ_z-distribution for, respectively, $[90_2/0_2/\pm45_2]_s$, $[0_2/90_2/\pm45_2]_s$ and $[(0/90)_2/(\pm45)_2]_s$. Similar τ_{xz}-distributions are shown, respectively, in Figures 12, 13 and 14. Since σ_z and τ_{xz} are predominant on both the mid-plane and the 45/-45 interface (in fact, both stresses are singular on the 45/-45 interface), it is not immediately clear in which plane edge delamination would occur.

Hence, an energy release rate calculation was subsequently followed. The energy release rate coefficient C_e for delamination in the mid-plane and in the 45/-45 interface was computed separately; and they are shown, respectively, in Figures 15 and 16. The corresponding C_T curves were not shown because of their relatively small values.

From the C_e-curves shown in Figures 15 and 16, it may now be inferred that a mode-I, mid-plane delamination would occur in all the three types of laminates. This is so because the computed C_e-curve for mid-plane delamination is higher than the C_e-curve for delamination in the 45/-45 interface plane.

To predict the actual onset load, the C_e-curve for mid-plane delamination must be used. Thus, as was done in the previous example, the minimum onset strain $\bar{e}_x$ can be calculated using Equations (6) and (7). The results are,

Laminate Type	Minimum Onset $\bar{\sigma}_x$
$[90_2/0_2/\pm 45_2]_s$	-303 Mpa (-44 ksi)
$[0_2/90_2/\pm 45_2]_s$	-352 Mpa (-51 ksi)
$[(0/90)_2/(\pm 45)_2]_s$	-407 Mpa (-59 ksi)

The corresponding experimental values may be determined from Figure 8, yielding the following respective load ranges: 290 - 310 Mpa; 331 - 358 Mpa; and 400 - 427 Mpa. The predicted results are, again, conforming with the experimental results.

In the example problems discussed in this section, the question regarding the size "a" of the assumed effective flaw was not dealt with directly. The assumption was simply that along the free edge of the laminate, the worst flaw has a size "a" which is at least equal or greater than a_m; and a_m is of the order of the layer thickness in which the assumed delamination is contained. The predicted onset load for delamination is thus the minimum possible load.

ONE - DIMENSIONAL GROWTH UNDER FATIGUE LOAD

It is well known that cyclic fatigue loads also induce sublaminate matrix cracks, including many forms of delamination growth. In fact, such cracks can be induced and propagated at fatigue stress levels much lower than the threshold stress determined statically. Generally, fatigue induced sublaminate cracks are similar to that induced by static load, although the respective mechanisms may be fundamentally different.

In a recent paper by Wang, et. al. [29], the formation process of transverse cracks in $[0/90]_s$ type laminates subjected to constant amplitude fatigue loading was investigated. It was demonstrated that given a fatigue load amplitude, say σ_f, a characteristic crack-density versus fatigue-time (cycles) relationship could be obtained experimentally, as well as analytically by means of a stochastic simulation model. Here, Wang, et. al. invoked once again the concept of effective flaw distribution. It was argued that inherent material flaws do propagate and coalesce under cyclic stress; however, the aggregate effect within a representative macro-volume may be described by the propagation of an assumed effective flaw having the size "a". In this context, Wang, et. al. assumed that the driving force that propagates "a" during each cycle of loading is related to the instantaneous flaw tip energy release rate $G(\sigma_f,a)$, which can be calculated as in the case of statically loaded problems. Specifically, a simple power law similar to that used for fine-grained metals [31] was used to describe the growth rate:

$$\frac{da}{dN} = \alpha \left[G(\sigma_f,a)/G_c\right]^p \qquad (8)$$

where N is the fatigue cycle and α and p are two disposable constants to be determined empirically.

It is noted that the quantity $G(\sigma_f,a)$ in Equation (8) already includes

the laminate stacking sequence, lamina thicknesses, laminate shape features, the individual flaw geometry, the nature of the applied load, etc. And, furthermore, the quantity G/G_c represents the crack-driving force relative to the material's resistance. Hence, the fatigue constants α and p are expected to be material dependent only. In particular, the exponent p is the most important parameter for the crack growth rate.

At this point, it seems appropriate to review briefly some related works concerning the growth rate equation (8) and the constants associated with that equation.

Wilkins [23] conducted fatigue delamination growth experiments using splitting cantiliver beams, and measured the growth rate as a function of the crack tip energy release rate $G(\sigma_f,a)$. Their test results support the power law for delamination growth, such as expressed in Equation (8). By taking the logarithm on both sides of (8), a linear relation between da/dN and $G(\sigma_f,a)$ is obtained; and the value of p is the slope of the straight line. Figure 17 shows one such experimentally measured da/dN versus $G(\sigma_f,a)$ plot from a mode-I delamination growth test. Figure 18 shows one for a mixed-mode delamination growth case. Wilkins' results generally confirm the adequacy of the assumed growth rate law for both mode-I and mixed-mode cases. However, the exponent p for mode-I growth is found to be two to three times larger than that for the mixed-mode case. Since the value of G/G_c in (8) is normally smaller than unity, a larger and positive p implies slower growth rate. Wilkins [23] suggested that mode-I delamination may be predominantly a static load failure, while mixed-mode delamination may be predominantly a fatigue load failure.

In an another study by Odom and Adams [32], the fatigue property of the 3501-06 epoxy resins was investigated. Two types of fatigue tests were performed: a tension-tension (R = 0.1) fatigue using a flat dog-bone coupon, and

a torsion-torsion fatigue using a round dog-bone coupon (also for R = 0.1). Both tests were conducted under ambient room temperature condition, and all tests were carried to the final failure of the specimen. The conventional S - N curves were obtained.

Let it be assumed that some dominant flaw of size "a" existed on the surface of the specimen, and it propagated stably under the cyclic stressing. The growth rate of the propagating flaw under the applied fatigue amplitude σ_f is governed by Equation (8). Since the energy release rate at the flaw tip can be expressed in terms of σ_f^2, Equation (8) may be written in the form

$$\frac{da}{dN} = \bar{\alpha}(a) \cdot (\sigma_f)^{2p} \tag{9}$$

For constant σ_f, a simple integration of (9) gives,

$$F(a) = N \cdot (\sigma_f)^{2p} \tag{10}$$

where F(a) is a known function of the flaw size "a". Assume that final failure occurred when $a \rightarrow a_{cr}$ at $N = N_{cr}$. The latter was measured experimentally and $F(a_{cr})$ became some constant. If the growth rate law (9) is true, then a linear relation between $\log(\sigma_f)$ and $\log(N_{cr})$ is obtained; the slope of the straight line yields the value of 2p.

Figure 19 shows the $\log(\sigma_f)$ versus $\log(N_{cr})$ plots for the tension and the torsion fatigue tests. These results, again, support the assumed growth rate law.

Note that failure in the tension fatigue case is of mode-I in nature. The associated fatigue exponent p is about 14, see Figure 19. On the other hand, failure in the torsional case is due mostly to shearing and some amount of axial tension due to a small pre-tension applied to the test specimen (see, Ref. [32]). The latter may be considered as a mixed-mode failure case. The

associated value for p is about 7.5. Although these values are found for the pure epoxy resin, they are consistent with those found for composites made of similar resins. Wilkins [23], for example, found the value of p for mode-I growth a range from 20 to 30, and for mixed-mode growth a range of 7 to 8. Wang, et. al. [29] used p = 20 in their mode-I transverse cracking simulation. Both used the same AS-fiber and the 3501-06 resin system.

Thus, it appears that the delamination growth rate equation (8) can be safely used to simulate it's growth behavior, although the exact physical mechanisms involved in the process could not be articulated. The latter remains outside the scope of the present paper.

Illustrative Example - Laminates Under Tension Fatigue.

As an illustrative example, consider the $[\pm 25/90]_s$ laminate discussed earlier in the static loading case. Recall that the static threshold stress for delamination was about 338 Mpa (49 ksi) and the growth was basically mode-I in nature. As the laminate was fatigue loaded at stress amplitudes below the static threshold stress, free edge delamination in the -25/90 interface was observed. This, of course, is a mixed-mode growth case.

Although the computed crack tip energy release rate $G(\sigma_f, a)$ is larger for mode-I growth than for mixed-mode growth, the latter is nevertheless predominant under cyclic stressing. This finding conforms with Wilkins' contention that mixed-mode delamination growth is usually a fatigue related failure mode.

For the considered laminate, the energy release rate coefficients C_e and C_T associated with delamination in the -25/90 interface are shown in Figures 6 and 7. Then, by means of the growth rate equation (8), the delamination growth can be predicted in terms of the fatigue amplitude σ_f and the cycle number N.

Figure 20 shows the experimental delamination growth curves under fatigue amplitudes σ_f = 207 Mpa (29 ksi) and 276 Mpa (40 ksi). The solid lines are the

corresponding predictions calculated based on G_c = 228 J/m^2 (1.3 in-lb/in^2) for mixed-mode growth, and the values for α and p were taken as

$$\alpha = 1.016 \text{ mm } (0.04 \text{ inch}); \qquad p = 8.3 \tag{11}$$

It is seen that the predictions are satisfactory. Note also that the value for p used here falls within the range found by Wilkins [23] and by Odom, et. al. [32].

Illustrative Examples - Laminates Under Compression Fatigue.

Consider further as examples the compressively loaded laminate family $[90_2/0_2/\pm45_2]_s$, $[0_2/90_2/\pm45_2]_s$ and $[(0/90)_2/(\pm45)_2]_s$. The respective static threshold stresses for edge delamination were determined previously at -303 Mpa (-44 ksi), -352 Mpa (-51 ksi) and -407 Mpa (-59 ksi); see Figure 8. When these laminates were tested under compression - compression fatigue loading (R = 0.1), stable growth of edge delamination was recorded at various cycle intervals (for details, see Ref. [3]). The delamination crack, however, occurred mostly in the -45/45 interface, indicating a mixed-mode growth case. This finding contrasts once again with the results of the static loading case where the edge delamination was essentially of mode-I (and confined in the laminate's mid-plane).

To simulate the mixed-mode growth, the energy release rate curves for edge delamination in the -45/45 interface were used in conjunction with the growth rate equation (8). Figure 21 shows a comparison between the experimental and the predicted results for the $[90_2/0_2/\pm45_2]_s$ and $[0_2/90_2/\pm45_2]_s$ laminates, both under σ_f = -221 Mpa (-32 ksi). The predicted results, shown in solid lines, were calculated using the same α and p values as listed in Equation (11). It is noted that the $[90_2/0_2/\pm45_2]_s$ laminate was the weaker under static loading, and it remained the weaker under the fatigue loading.

Similarly, Figure 22 shows a comparison between the $[0_2/90_2/\pm45_2]_s$ and the $[(0/90)_2/(\pm45)_2]_s$ laminates when both were loaded under σ_f = -278 Mpa (-40 ksi). Note that the latter laminate displayed a distinctly stronger resistance against delamination, as it also did when under statically applied load.

All these physical features pertaining to the onset and growth of delamination could be predicted by the energy model. This is particularly remarkable considering the scattering nature of the fatigue results. More comparative studies using other laminate geometries and/or other loading combinations have been reported in Ref. [30] and [33].

TWO - DIMENSIONAL GROWTH PROBLEMS

In the preceding sections, the energy release rate method has been applied to simulate a number of free edge delamination growth problems. The laminates studied were so designed and loaded as to induce delamination growth without significant interaction with other cracking modes. Furthermore, the delamination was confined to grow uniformly along the straight edge of the test coupon, so it could be assumed as one-dimensional, self-similar growth. Under this assumption, the kinematics of the crack propagation is much simplified, with the crack front being represented by a point known as the crack-tip, and the crack size having the magnitude "a". This simplification has made a two-dimensional stress field solution possible, from which the crack-tip energy release rate function $G(\bar{\sigma},a)$ could be calculated by a numerical technique.

Generally speaking, one-dimensional delamination growth is a very special case, and it happens only under ideally controlled conditions. Most of the problems encountered in practice are localized events usually caused by local defects. The growth of localized delamination is almost always multi-directional in nature.

For example, consider a laminate having a small through-hole. Upon loading, localized delamination may be induced near the curvilinear edge of the hole. In this case, the crack front will be some line-contour, and the associated growth will be two-dimensional. The instantaneous crack size "a" is now the delaminated area, which will have both a magnitude and a definite shape contour.

Clearly, a three dimensional stress field solution is needed in order to calculate the crack front energy release rate $G(\bar{\sigma},a)$, with "a" being some definite line contour.

In a separate effort, Wang, Kishore and Li [35] developed a 3-D finite element routine in which Irwin's crack-closure concept was incorporated to

calculate the crack front energy release rate along a prescribed delamination contour. Utilizing this 3-D finite element routine, several two-dimensional crack growth problems have been simulated. The following section examines one such problem.

Illustrative Example - Growth From A Pre-Planted Delamination.

Earlier in this paper, compression induced free edge delamination in three similar quasi-isotropic laminates was examined and modeled as one-dimensional growth problems, see Figure 8. One of the laminates, $[0_2/90_2/\pm45_2]_s$, was later tested with an implanted delamination at it's mid-plane, see insert in Figure 23. The experimental details regarding the implantation and test procedures were reported in Ref. [3]. Figure 23 shows the test results from three specimens with the implant. When compared with specimens without the implantation, the laminates with the implant show a strikingly different growth behavior. Specifically, the laminates with the implant underwent a contoured (2-D) delamination growth, while the ones without an implant experienced more or less uniform (1-D) free edge delamination. Although the contoured growth was much more slow and stable, it's early initiation had actually led to early laminate failure, see Figure 23.

In order to predict the onset of the contoured delamination, the 3-D finite element simulation routine developed in Ref. [35] was used.

But before preceding with the growth simulation, a stress analysis was performed with emphasis placed at the location where the most severe stress concentration is present. This location is the interface corner where the implanted delamination front intersects the free edge of the test coupon, see Figure 24, labeled "interface corner".

It is recalled that the laminates without the implant developed a tensile interlaminar σ_z stress near the laminate free edge. And, for a far-field strain

$\bar{e}_x = -10^{-6}$ the value of σ_z near the free edge (acting on the mid-plane) is about 14 kpa (2 psi). On the other hand, the laminates with the implant developed a strikingly different σ_z-distribution in the same laminate mid-plane, see Figure 24. The stress near the "interface corner" is in fact singular in nature; the actual value of σ_z near the vicinity is several times larger.

In fact, σ_z is not the only stress which is amplified at this point (the two interlaminar shear stresses are zero due to lamination symmetry). Figure 25 shows the in-plane stresses σ_x, σ_y, and τ_{xy} along with σ_z that are acting in the 45-layer adjacent to the laminate mid-plane. It is seen that all of the stresses are severely concentrated near the "interface corner" point. These stresses, particularly σ_z, are obviously responsible for the observed early growth of contoured delamination.

Returning to predicting the associated delamination growth, one must begin with the calculation of the crack front strain energy release rate. Since the expected delamination will start from the "interface corner" point, and grow with a certain contoured front, a reasonable sequence of nodal release may be prescribed. For example, Figure 26 (a) shows one possible nodal release sequence which simulates the delamination growth process (the node numbers represent the order of nodal release). The computed energy release rate coefficient C_e as a function of the correspondingly delaminated area is shown in Figure 26 (b).

It is seen that the delamination growth is most energetic along the implant edge as compared to the energy released along the laminate free edge. As the delaminated area becomes larger, the available energy release rate becomes smaller. This implies that the growth process is essentially stable, as it has been observed in the experiment, see Figure 23.

To determine the onset load, the maximum value of C_e in Figure 26 (b) will be used in order to predict the minimum onset load. By disregarding the thermal

effect on delamination (because C_T is relatively small), the maximum strain energy release rate can be expressed by,

$$G_{max} = (C_e)_{max} (\bar{e}_x)^2 t \qquad (12)$$

where the value of $(C_e)_{max}$ corresponds to the release at node 6, see Figure 26.

Using G_c = 175 J/m^2 (1,0 in-lb/in^2) for mode-I delamination, and t = 0.13 mm (0.005 in.), the calculated minimum onset load (the applied far-field strain $\bar{e}_x$) is approximately,

$$(\bar{e}_x)_{min} = 2890 \times 10^{-6} \qquad (13)$$

For the laminate considered, the axial stiffnes is $\bar{E}_x$ = 50.1 Gpa (7.27 msi); it follows that the predicted (minimum) onset far-field laminate stress is

$$(\bar{\sigma}_x)_{min} = 145 \text{ Mpa } (21.0 \text{ ksi}) \qquad (14)$$

This predicted value is just about the same as the experimental value which can be extracted from Figure 23.

CONCLUDING REMARKS

In this paper, the energy release rate concept was applied to describe the initiation and growth processes in some of the most prevalent matrix cracks found in composite laminates. Several experimental case studies were used in order to illustrate the analytical models. At the conclusion of this paper, the following remarks are in order:

1. For matrix cracks such as delamination, the energy release rate method can be applied within the frame work of ply elasticity and the classical fracture mechanics. To do so, all variables associated with the analytical model must be defined or determined at the material ply level.

2. For self-generated matrix cracks (cracks caused by inherent material flaws), a concept of "effective" flaw can be used in place of the conventional strength concept. The new concept is consistent with the fundamental postulations in the classical fracture mechanics. And, by defining it as an "effective" basic material property, the concept is also consistent with the assumptions of ply elasticity (that all material properties are defined at the ply level). This concept provides the necessary arguement for multiple crack formations observed in laminates, for which the conventional constant ply strength concept cannot.

3. One-dimensional delamination growth, such as uniformly delaminated free edge, is a special case. Most practical problems are in a class of localized dalamination whose growth behavior is two-dimensional in nature. The same energy release rate concept can still be applied, provided a three dimensional stress solution technique is made available for the calculation of the energy release rate along the contoured delamination front. This topic is still new; future research is required.

4. Experimental results from fatigue tests seem to suggest that mode-I delamination is generally static load related failure, while mixed-mode delamination is fatigue load related failure. Correlations between test results and analysis also reveal this tendency. The fundamental mechanisms of fatigue failure remain yet to be investigated.

5. On the basis of a limitted fatigue delamination data, a simple power law for the growth rate was applied in several case studies. Though still tentative in nature, the growth law seemed to show a considerable generality for fatigue growth simulation. Again, more research is neened here.

REFERENCES

[1] Pagano, N. J. and Pipes, R. B.,"The Influence of Stacking Sequence On Laminate Strength," Journal of Composite Materials, Vol. 5, Jan. 1971, p. 50.

[2] Bjeletich, J. G., Crossman, F. W. and Warren, W. J.,"The Influence of Stacking Sequence On Failure Modes in Quasi-isotropic Graphite-Epoxy Laminates," in Failure Modes In Composites - IV, American Institute of Metallurgical Engineers, Washington, D. C., 1979, p. 118.

[3] Wang, A. S. D. and Slomiana, M., "Fracture Mechanics of Delamination - Initiation and Growth," NADC-TR-79056-60, Naval Air Development Center, Warminster, PA., Jan. 1982.

[4] Pipes, R. B. and Pagano, N. J.,"Interlaminar Stresses in Composite Laminates Under Uniform Axial Tension," Journal of Composite Materials, Vol. 4, Oct. 1970, p. 538.

[5] Tang, S.,"Interlaminar Stresses of Uniformly Loaded Rectangular Composite Plate," Journal of Composite Materials, Vol. 10, Jan. 1976, p. 69.

[6] Wang, A. S. D. and Crossman, F. W.,"Some New Results on Free Edge Effects in Symmetric Composite Laminates," Journal of Composite Materials, Vol. 11, Jan. 1977, p. 92.

[7] Wang, S. S. and Choi, I.,"Boundary Layer Effects in Composite Laminates," Part 1 and Part 2, Journal of Applied Mechanics, Vol. 49, Sep. 1982, p. 541.

[8] Rodini, B. T. and Eisenmann, J. R.,"An Analytical and Experimental Investigation of Edge Delamination in Composite Laminates," in Fibrous Composites in Structural Design, Ed. E. M. Lenoe, et al, Pleum Press, N. Y., 1978, p. 441.

[9] Crossman, F. W. and Wang, A. S. D.,"The Dependence of Transverse Cracks and Delamination on Ply Thickness in Graphite-Epoxy Laminates," STP 775, Damage in Composite Materials, American Society for Testing and Materials, 1982, p. 118.

[10] Wang, A. S. D. and Crossman, F. W.,"Initiation and Growth of Transverse Cracks and Edge Delamination in Composite Laminates," Part 1. An Energy Method, Journal of Composite Materials, Vol. 14, No. 1, 1980, p. 71.

[11] Crossman, F. W.,Warren, W. J., Wang, A. S. D. and Law, G. E.,"Initiation and Growth of Transverse Cracks and Edge Delamination in Composite Laminates," Part 2. Experimental Correlation, Journal of Composite Materials, Vol. 14, No. 1, 1980, p. 88.

[12] Wang, A. S. D.,"Growth Mechanisms of Transverse Cracks and Ply Delamination in Composite Laminates," Proceedings, International Conference on Composite Materials, Vol. 1, Paris, 1980, p. 170.

[13] Wang, A. S. D.,"Fracture Mechanics of Sublaminate Cracks in Composite Laminates," in Characterization, Analysis and Significance of Defects in Composite Materials, Conference Proceeding No. 355, NATO Advanced Group on Aeronautic Research and Development, London, 1983, p. 15-1.

[14] Wang, A. S. D. and Crossman, F. W.,"Fracture Mechanics of Sublaminate Cracks," Technical Report, Contract No. F-49620-79-C-0206, Air Force Office of Scientific Research, Washington, D. C. 1982.

[15] Tetelman, A. S. and McEvily, A. J., Jr.,"Fracture of Structural materials," John Wiley and Sons, New York, 1967.

[16] Tsai, S. W. and Hahn, H. T.,"Introduction to Composite Materials," Technomics, Stamford, CT, 1980.

[17] Muskhelishvili, N. I.,"Some Basic Problems From the Mathematical Theory of Elasticity," Noordhoff, Holland, 1953.

[18] Snedden, I. N.,"Integral Transform Methods," in Methods of Analysis and Solutions of Crack Problems, Noordhoff, Holland, 1973, p. 315.

[19] Rice, J. R.,"A Path Independent Integral and Approximate Analysis of Strain Concentration by Notches and Cracks," Journal of Applied Mechanics, Transactions of the American Society of Mechanical Engineers, Series E, Vol. 90, 1968, p. 379.

[20] Bucci, R. J., Paris, P. C., Landis, J. D. and Rice, J. R.,"J-Integral Estimation Procedures," in STP 514, Fracture Thoughness, Part II, American Society for Testing and Materials, 1972, p. 40.

[21] Irwin, G. R.,"Fracture" in Handbuch der Physik, Vol. 5, Springer-Verlag, Berlin, 1958, p. 551.

[22] Rybicki, E. F. and Kanninen, M. F.,"A Finite Element Calculation of Stress Intensity Factors by A Modified Crack-Closure Integral," Engineering Fracture Mechanics, Vol. 9, 1977, p. 931.

[23] Wilkins, D. J.,"A Comparison of the Delamination and Environmental resistance of A Graphite-Epoxy and A Graphite-Bismaleimide," Technical Report NAV-GD-0037, Naval Air Systems Command, Washington, D. C., Sept. 1981.

[24] Cullen, J. S.,"Mode-I Delamination of Unidirectional Graphite Epoxy Composite Under Complex Load Histories," M. S. Thesis, Texas A & M University, College Station, TX. 1981.

[25] Williams, D.,"Mode-I Transverse Cracking in An Epoxy and A graphite Fiber Reinforced Epoxy," M. S. Thesis, Texas A & M University, College Station, TX. 1981.

[26] Vanderkley, P. S.,"Mode-I and Mode-II Delamination Fracture Thoughness of A Unidirectional Graphite Epoxy Composite," M. S. Thesis, Texas A & M University, College Station, TX. 1981.

[27] Wilkins, D. J., Eisenmann, J. R., Camin, R. A., Margolis, W. S. and Benson, R. A.,"Characterizing Delamination Growth in Graphite Epoxy," in STP 775, Damage in Composite Materials, American Society for Testing and Materials, 1982, p. 168.

[28] Wang, A. S. D., Kishore, N. N. and Feng, W. W.,"On Mixed-mode Fracture in Off-Axis Unidirectional Graphite-Epoxy Composites," Proceedings of International Conference on Composite Materials IV, Vol. 1, Japan Society for Composite Materials, Tokyo, 1982. p. 599.

[29] Wang, A. S. D., Chou, P. C. and Lei, S. C.,"A Stochastic Model for the Growth of Matrix Cracks in Composite Laminates," in Advances in Aerospace Structures, Materials and Dynamics, American Society of Mechanical Engineers, N. Y. 1983, p. 7.

[30] Wang, A. S. D., Chou, P. C., Lei, S. C. and Bucinell, R.,"Cumulative Damage Model for Advanced Composite Materials," Technical Report, for Contract No. F-33615-80-C-5039, Air Force Wright Aeronautical Laboratories, Dayton, OH. Aug. 1983.

[31] Dieter, G. E.,"Mechanical Metallurgy," 2nd. Ed. McGraw Hill, New York, 1976, p. 419.

[32] Odom, E. M. and Adams, D. E.,"A Study of Polymer Matrix Fatigue Properties," NADC-TR-83053-60, Naval Air Development Center, Warminster, PA. Sep. 1983.

[33] Slomiana, M.,"Fracture Mechanics of Delamination in Graphite Epoxy Laminates Under Compression," Ph.D. Thesis, Drexel University, Philadelphia, PA. 1984.

[34] Crossman, F. W., Warren, W. J. and Wang, A. S. D.,"Influence of Ply Thickness On Damage Accumulation and Final Failure," in Advances in Aerospace Structures, Materials and Dynamics, American Society of Mechanical Engineers, New York, 1983, p. 215.

[35] Wang, A. S. D., Kishore, N. N. and Li, C. A.,"A Three Dimensional Finite Element Analysis of Delamination Growth in Composite Laminates," Part 2, The Computer Code KSAP, User's Manual, NADC-84018-60, Naval Air Development Center, Warminster, Pa., Nov., 1983.

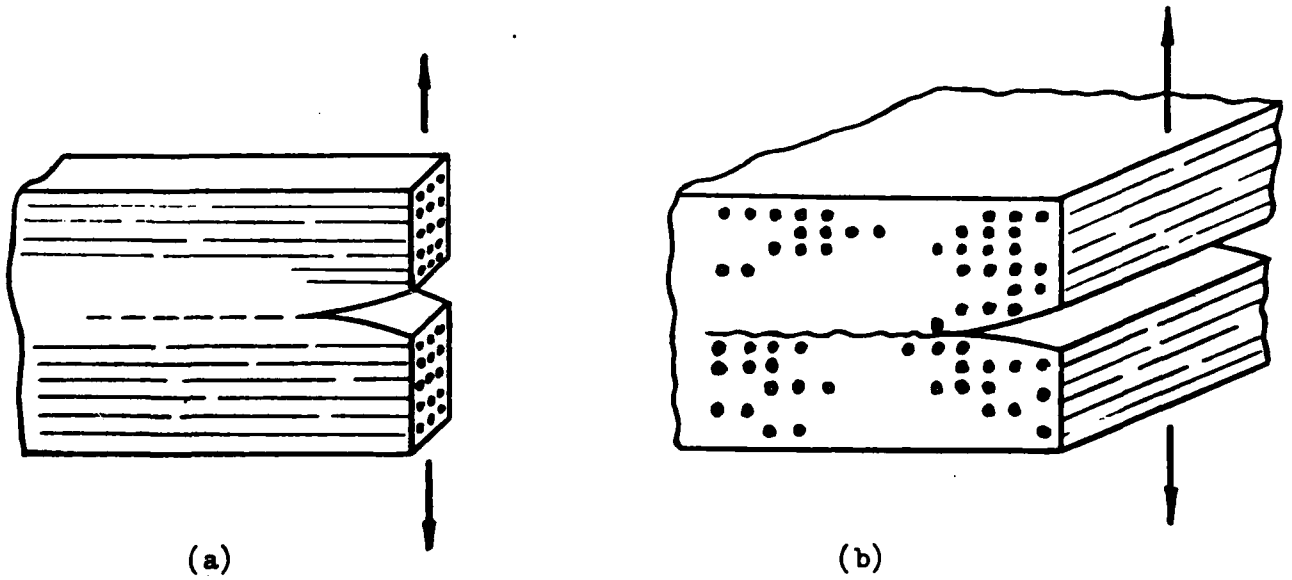

Figure 1. Mode-I Delamination Growth Direction; (a) In the Direction of the Reinforcing Fibers; (b) In the Direction Normal to the Reinforcing Fibers.

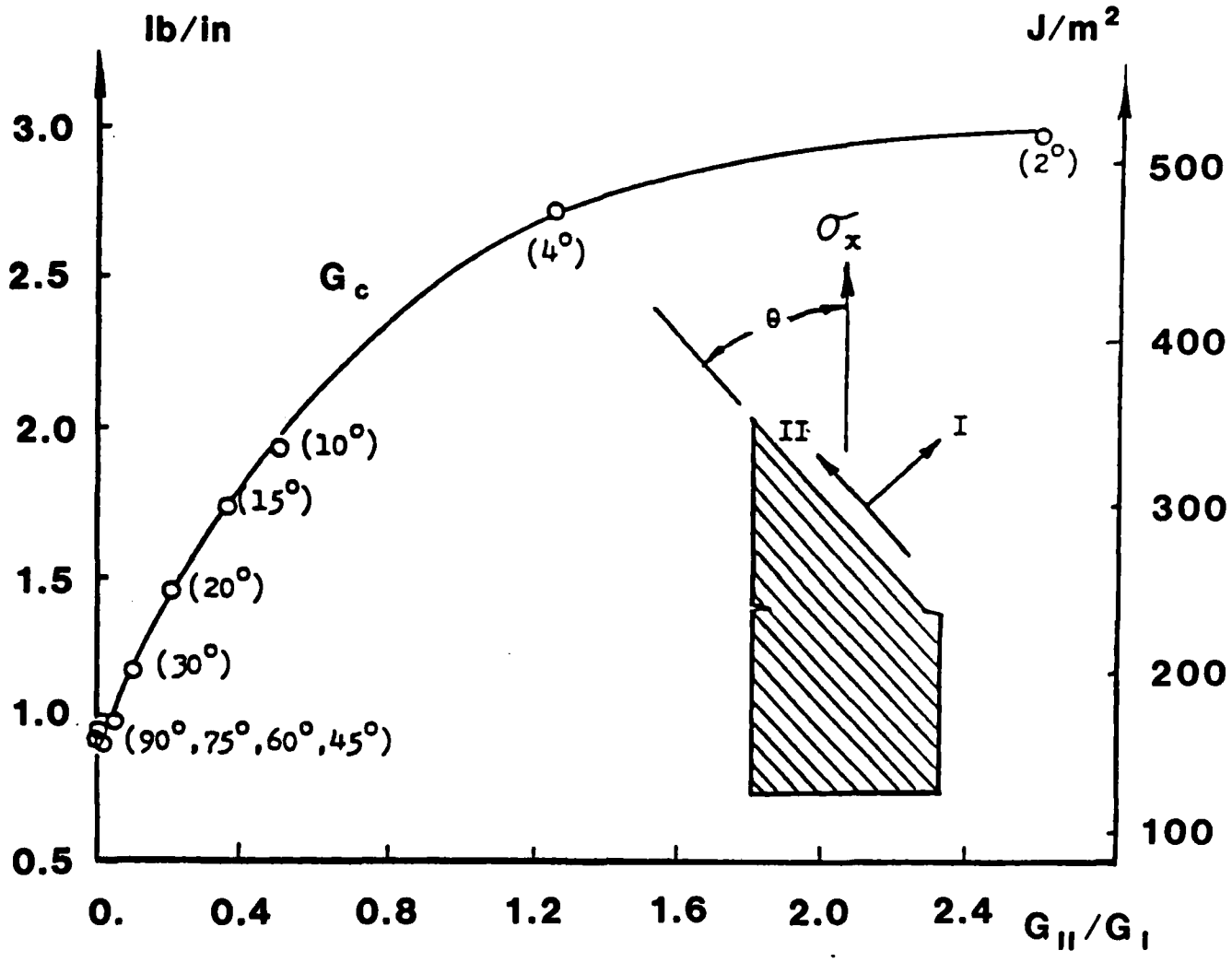

Figure 2. Critical Energy Release Rate for Mixed-Mode Delamination in Graphite-Epoxy Laminate. Ref. [28].

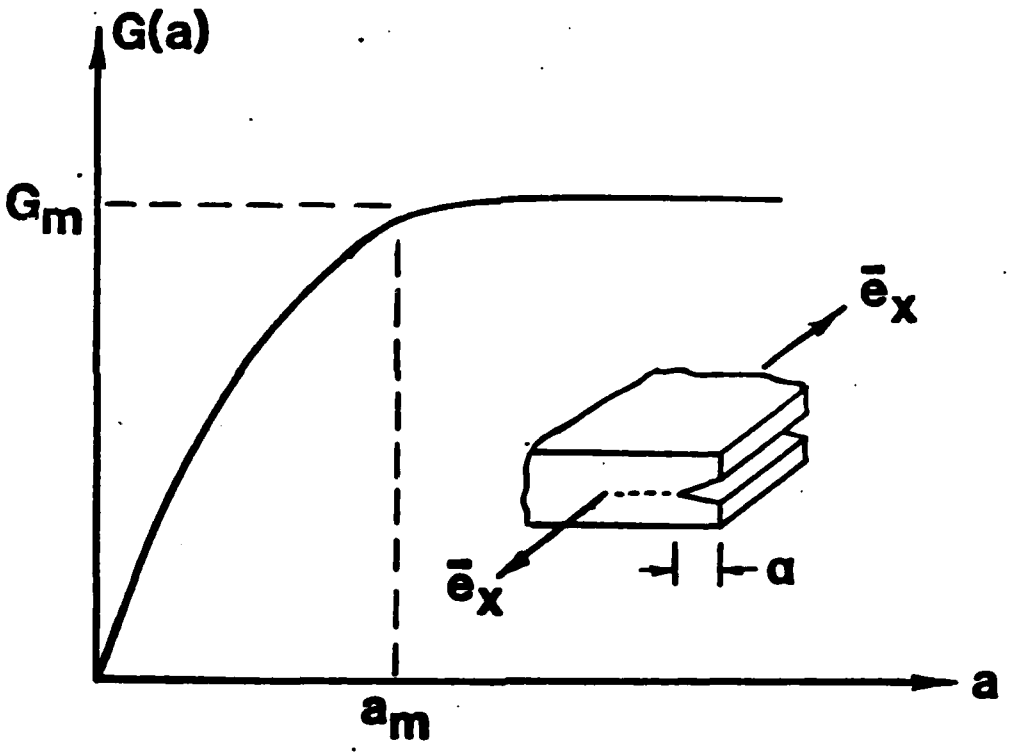

Figure 3. Shape of the Energy Release Rate Function G(a) for Free Edge Delamination Growth.

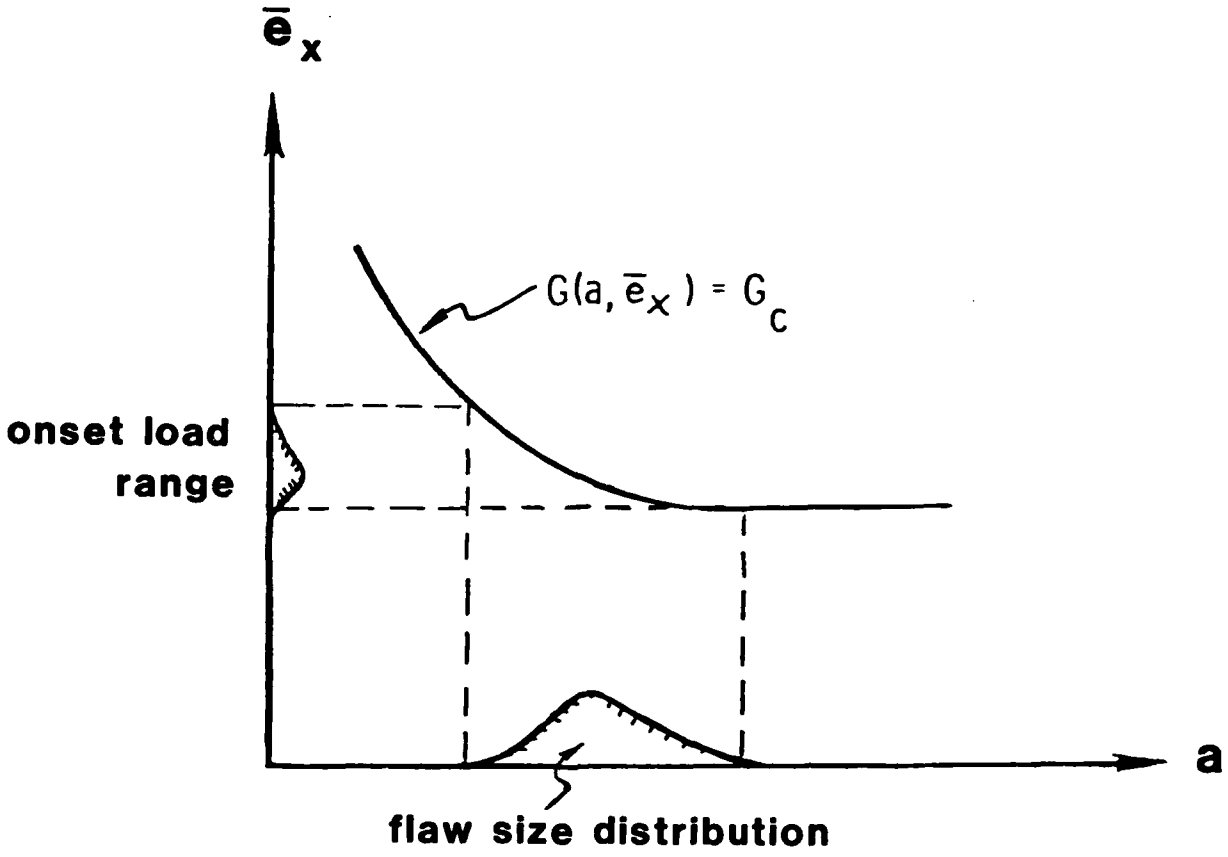

Figure 4. Rationale For Predicting the Onset Load of Delamination According to Fracture Mechanics Criterion.

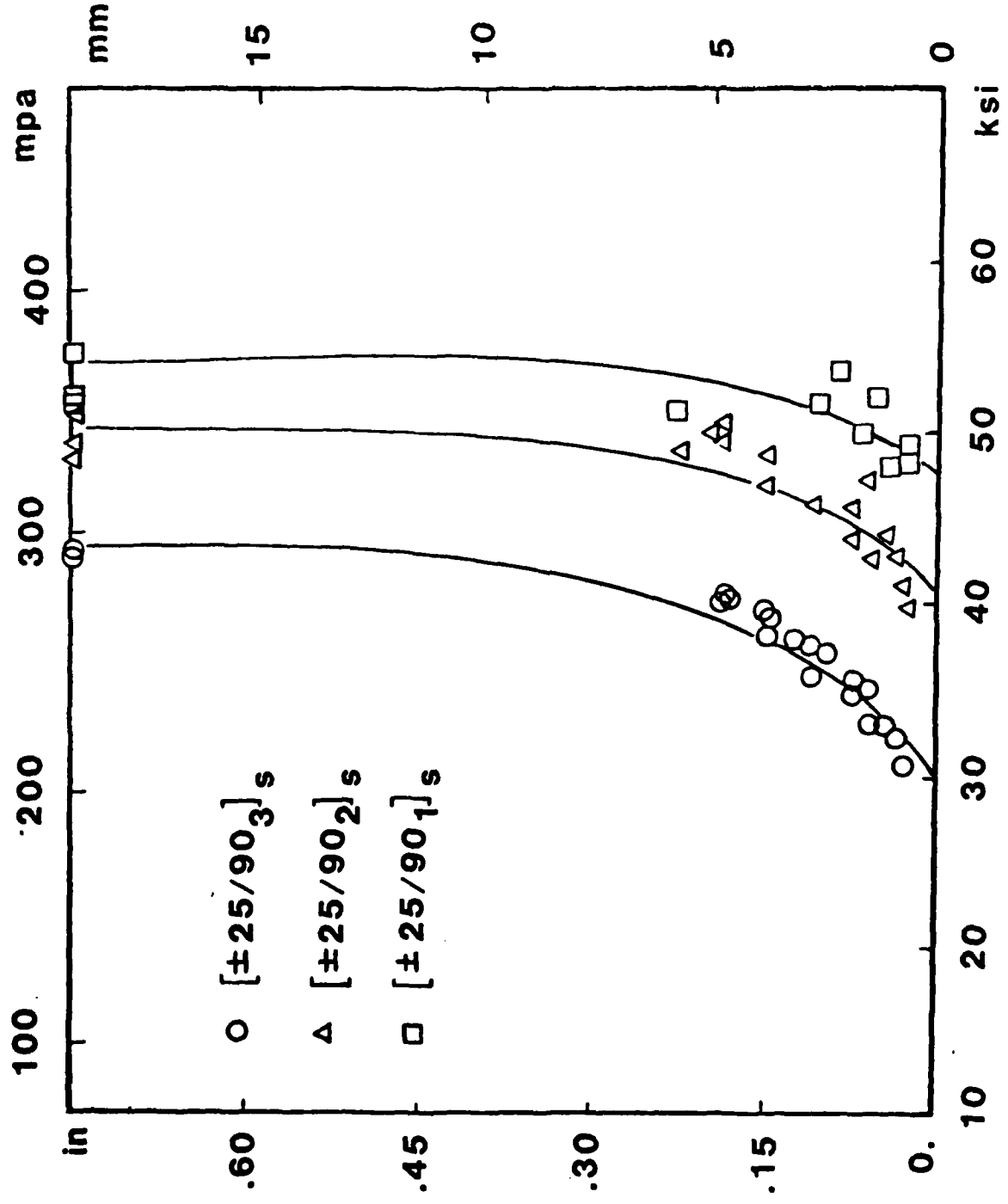

Figure 5. Experimental Edge Delamination Growth Curves Under Uniaxial Tension. Ref. [30].

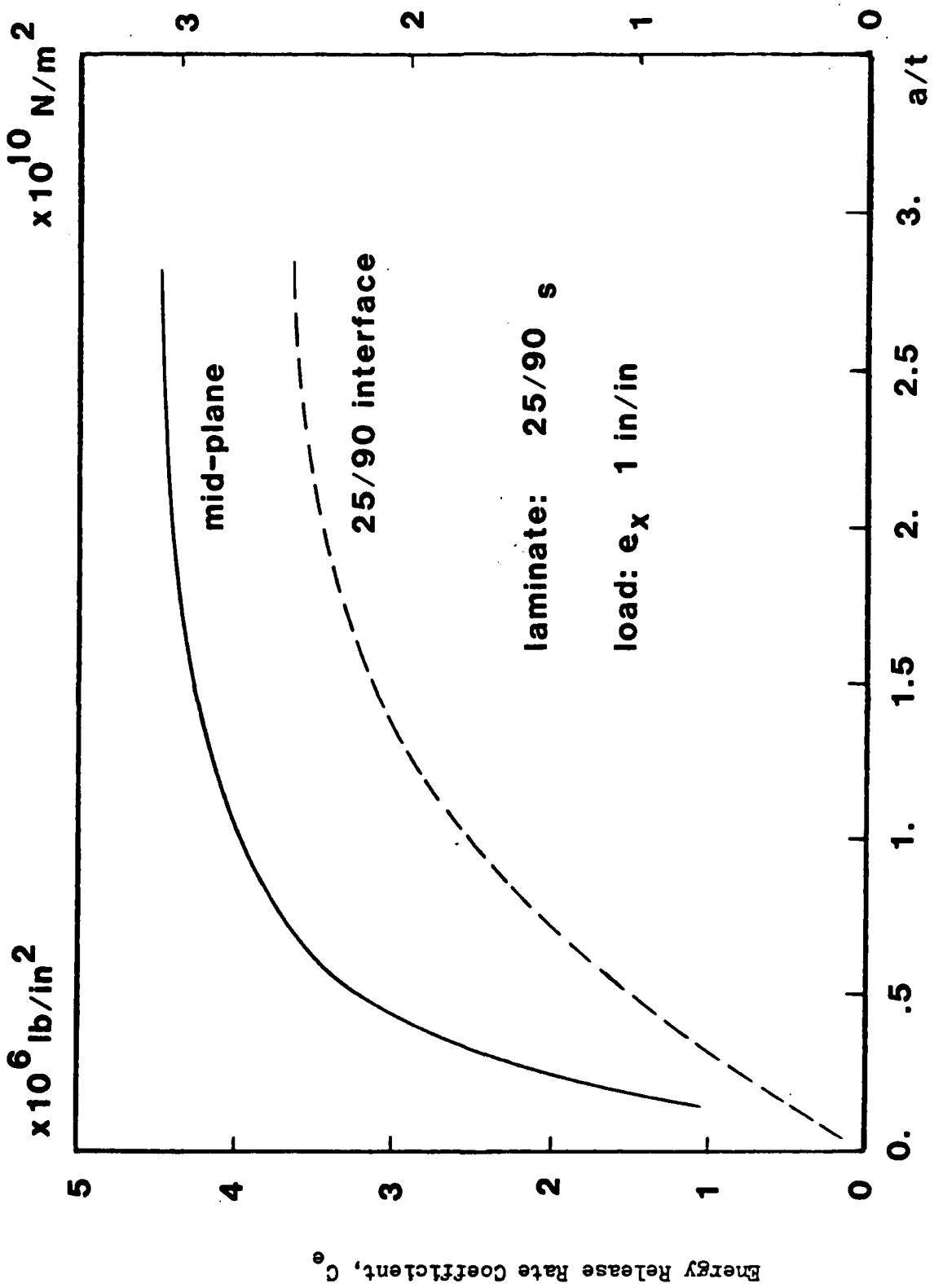

Figure 6. Energy Release Rate Coefficient Function C_e for Delamination in $[\pm 25/90]_s$ Laminate

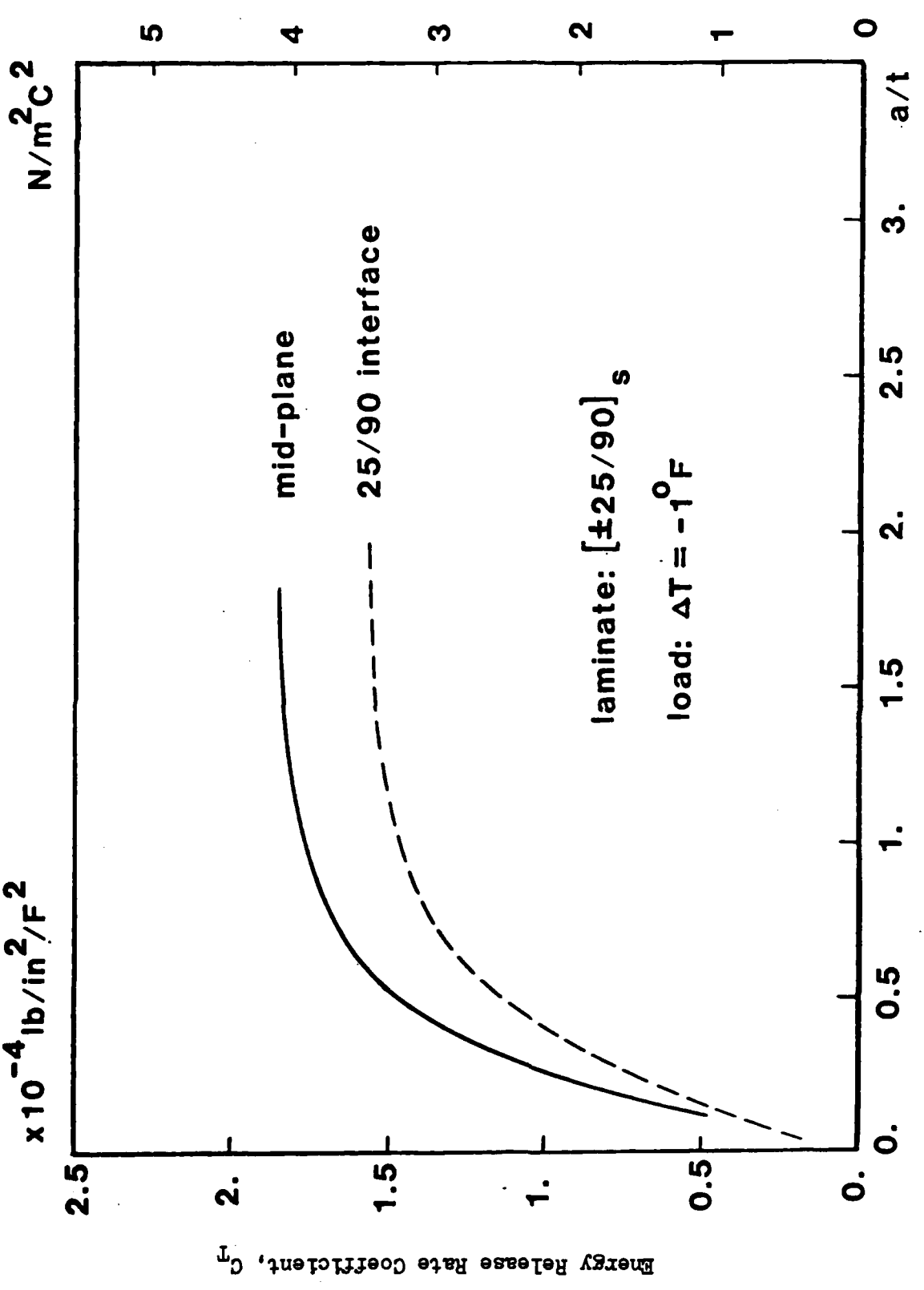

Figure 7. Energy Release Rate Coefficient Function C_T for Delamination in $[\pm 25/90]_s$ Laminate

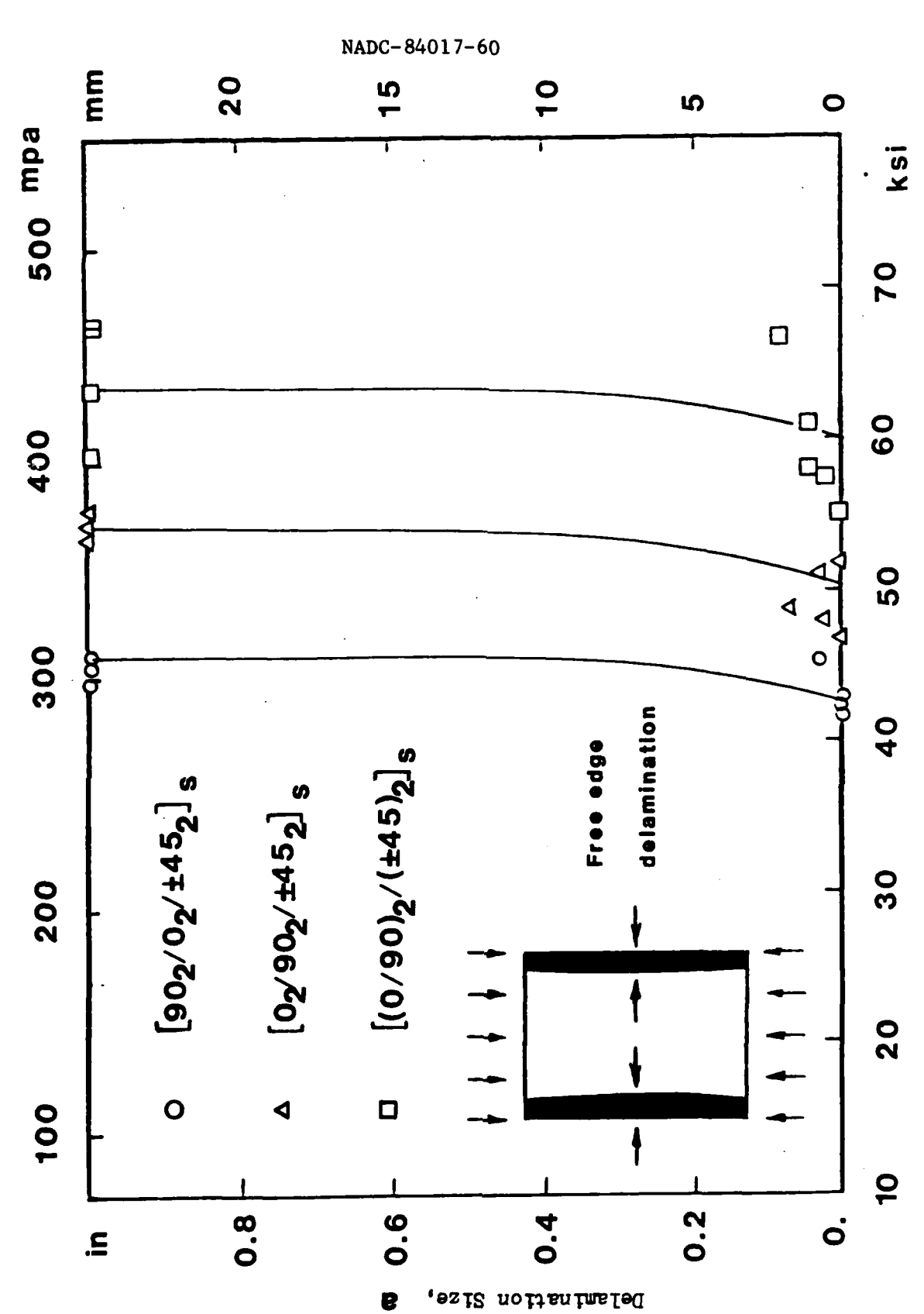

Figure 8. Experimental Edge Delamination Growth CurvesUnder Uniaxial Compression. Ref. [3].

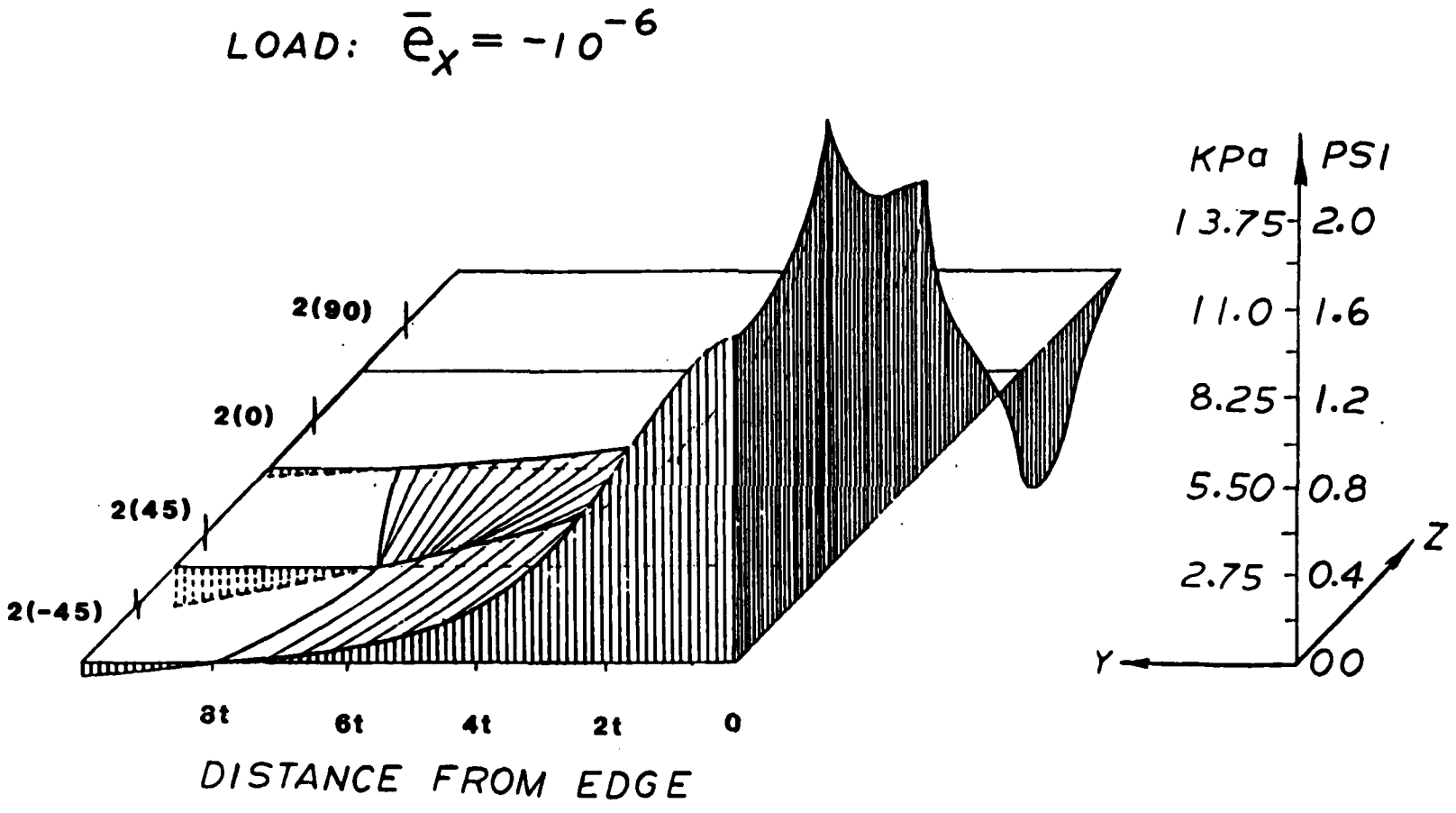

Figure 9. Through-Thickness Distribution for the Interlaminar Stress σ_z Near Free Edge

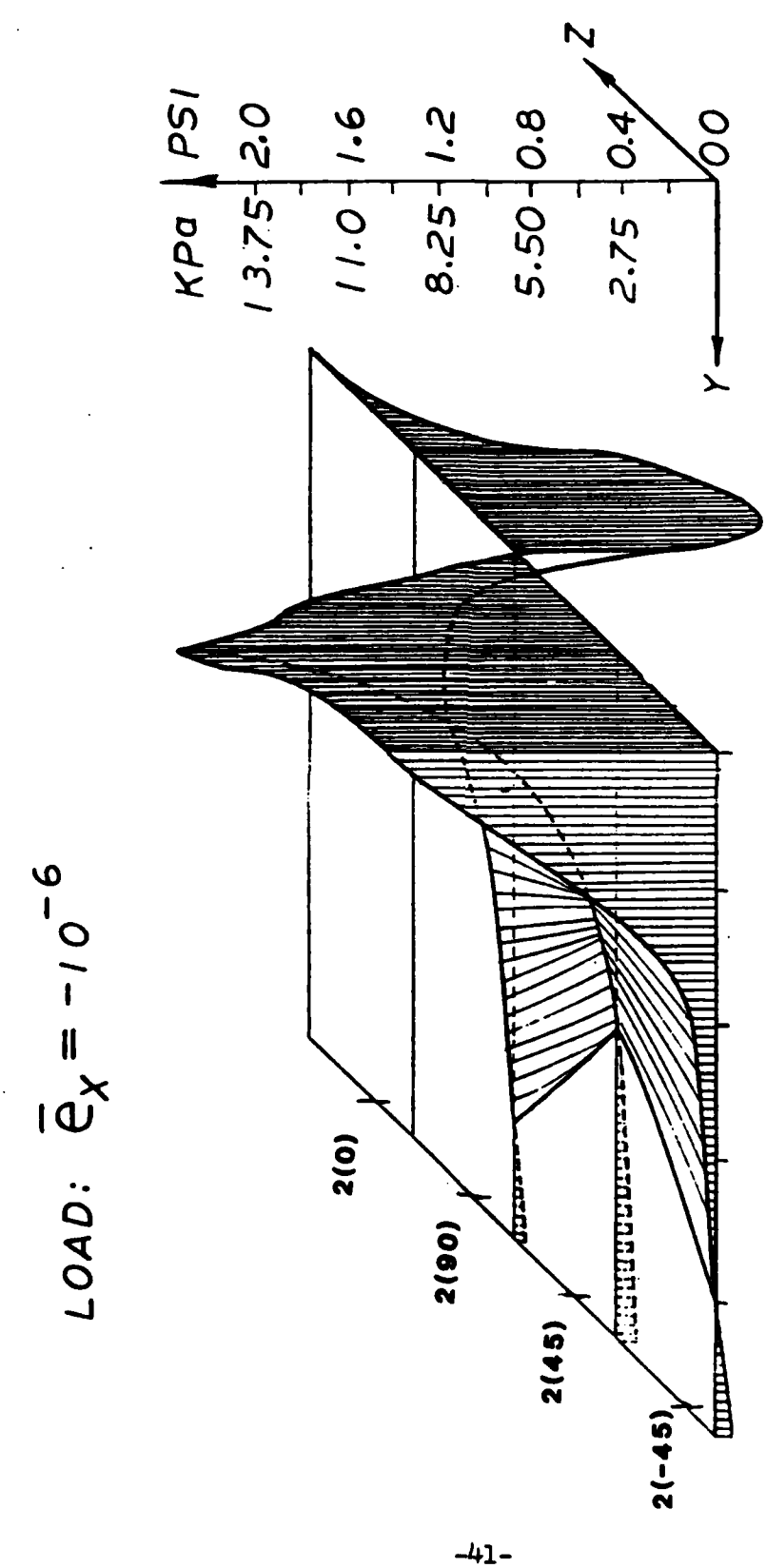

Figure 10. Through-Thickness Distribution for the Interlaminar Stress σ_z Near Free Edge.

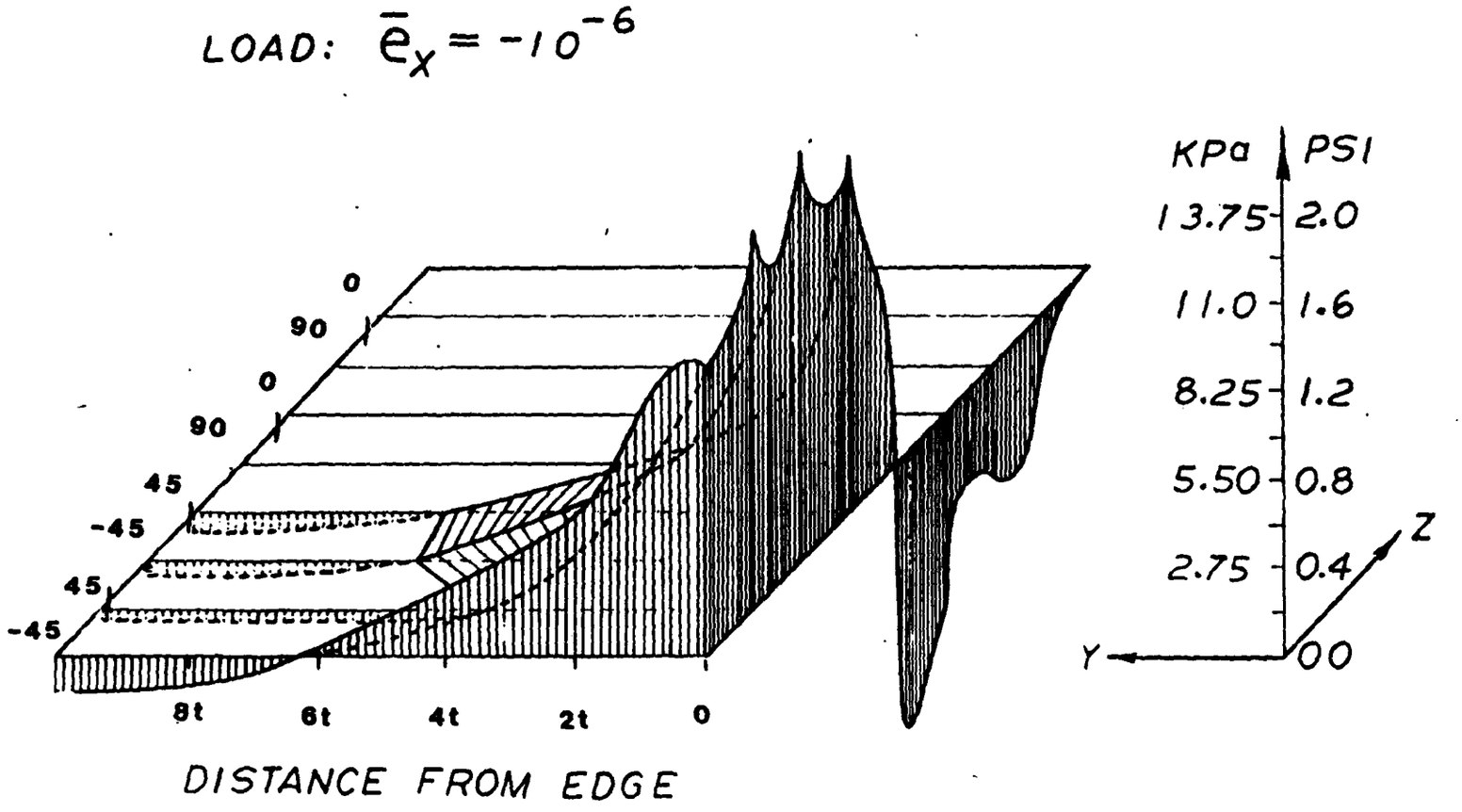

NADC-84017-60

Figure 11. Through-Thickness Distribution for the Interlaminar Stress σ_z Near Free Edge.

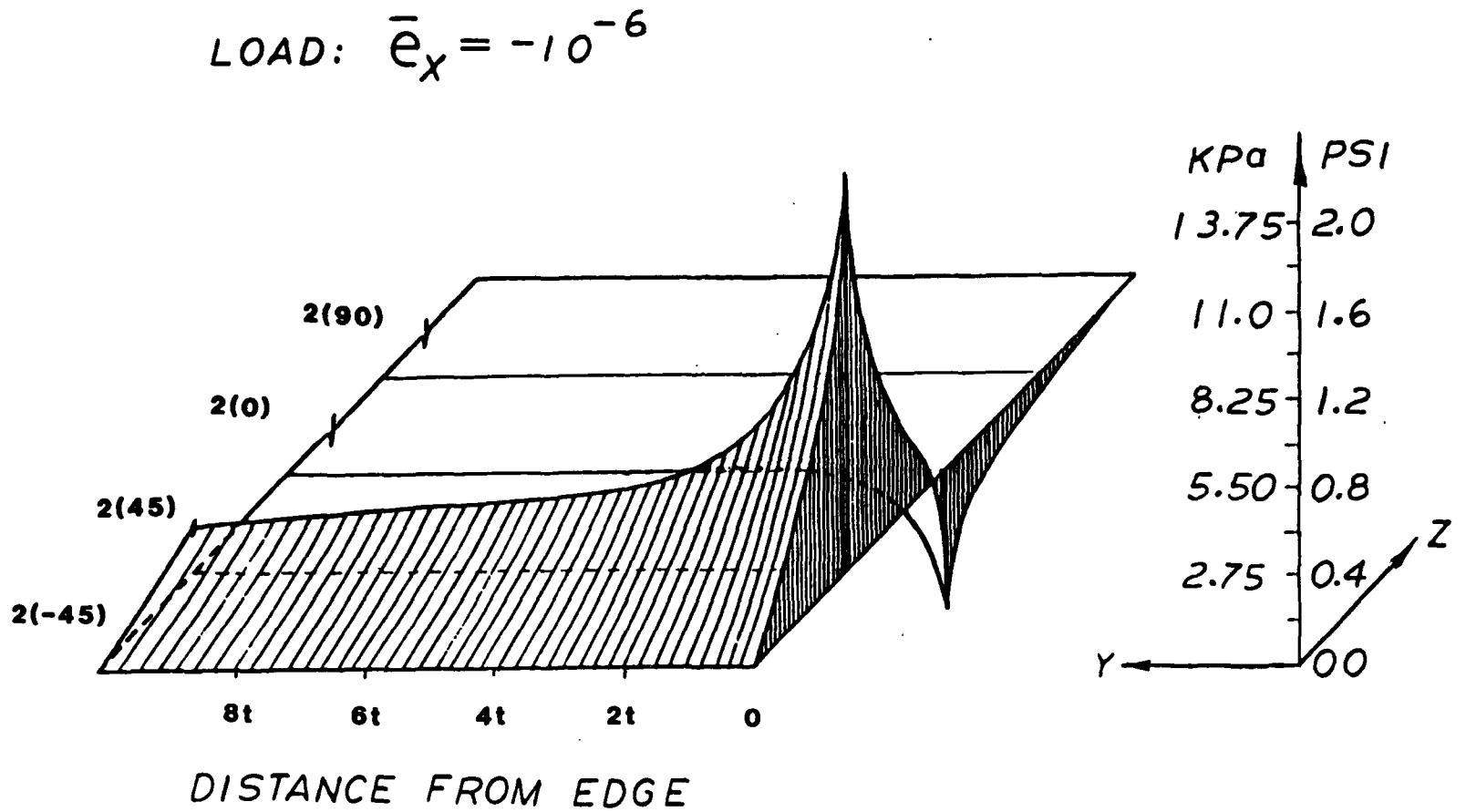

Figure 12. Through-Thickness Distribution for the Interlaminar Stress τ_{xz} Near Free Edge.

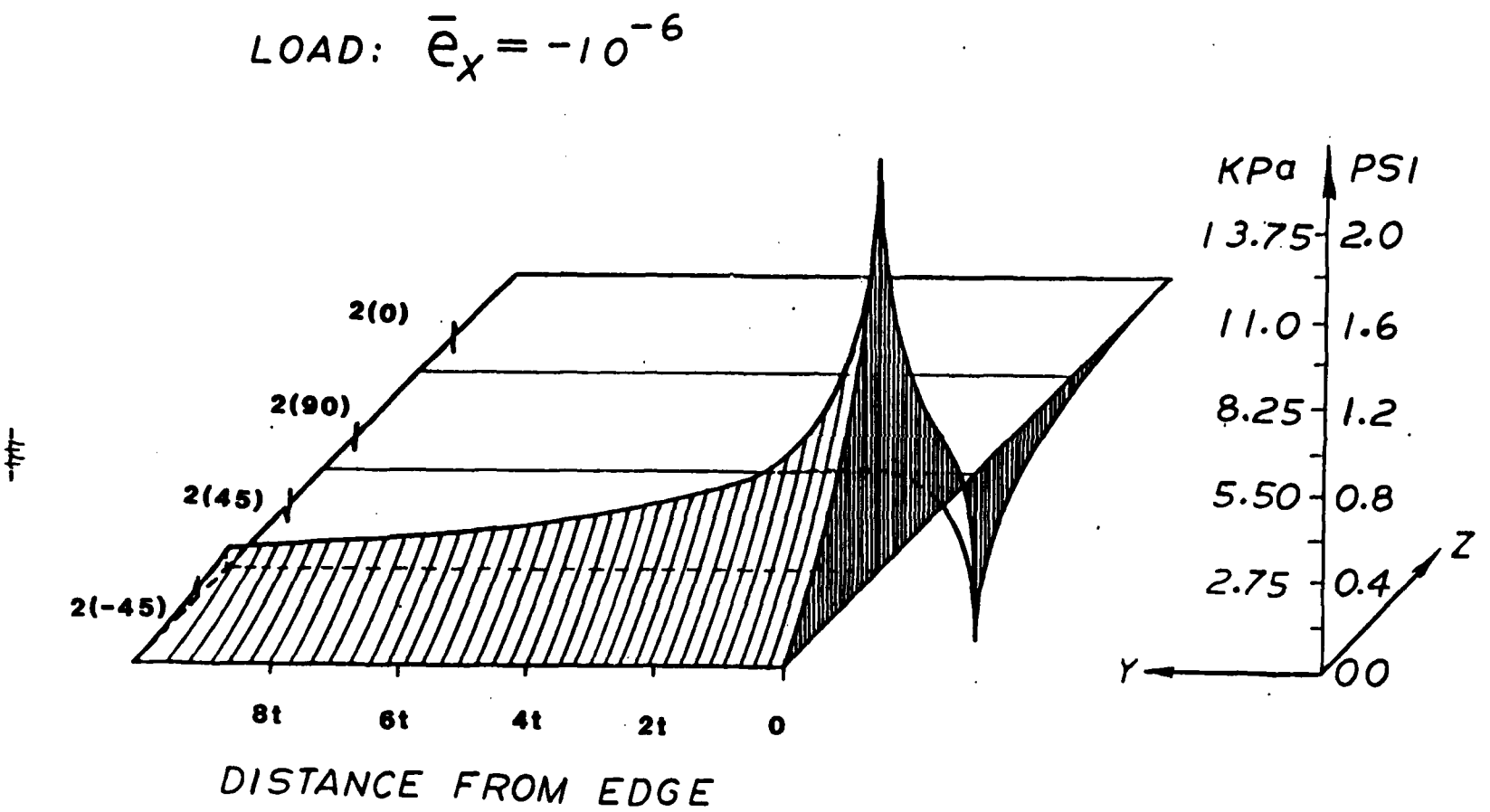

NADC-84017-60

Figure 13. Through-Thickness Distribution for the Interlaminar Stress τ_{xz} Near Free Edge.

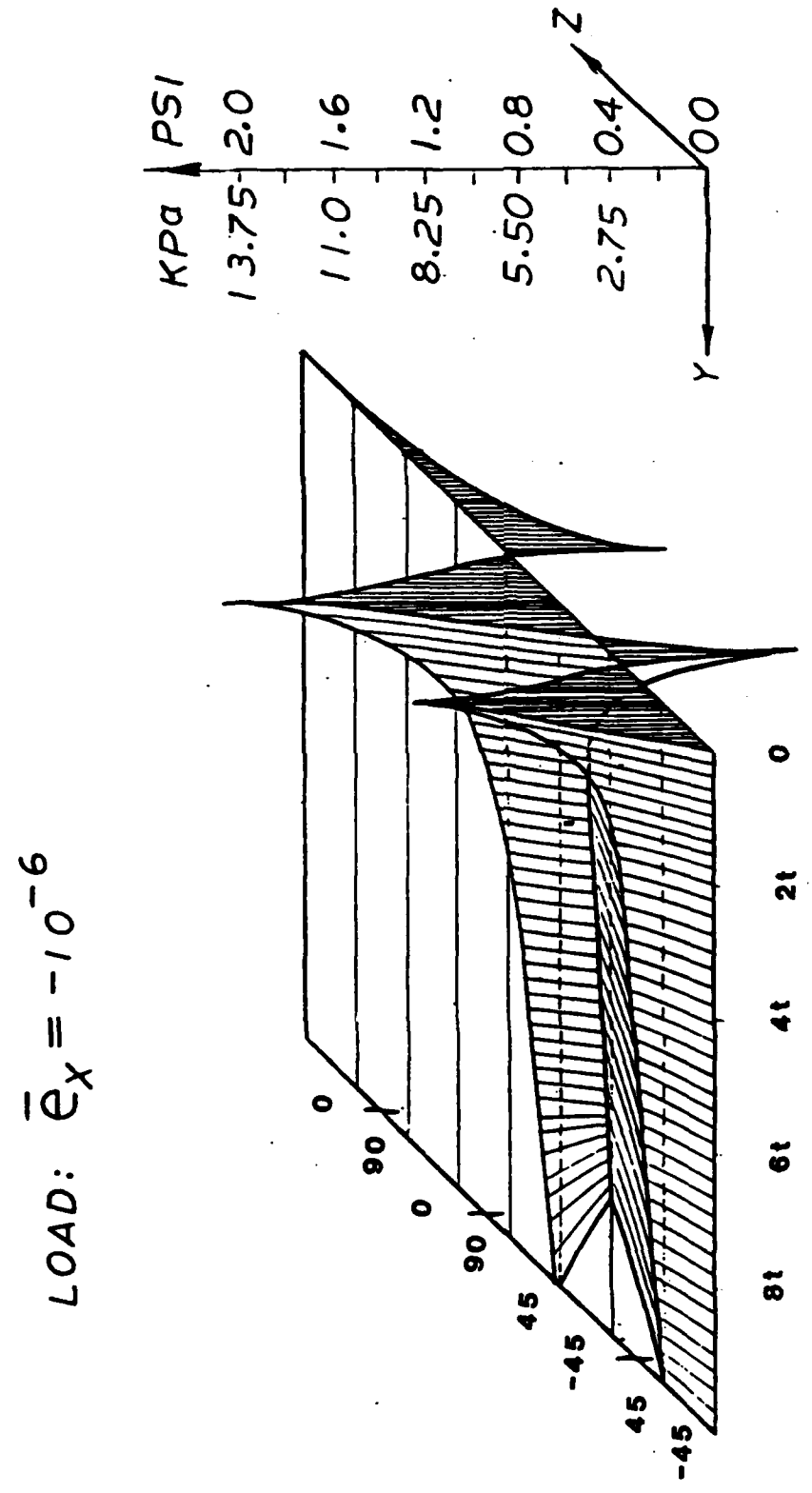

Figure 14. Through-Thickness Distribution for the Interlaminar Stress τ_{xz} Near Free Edge.

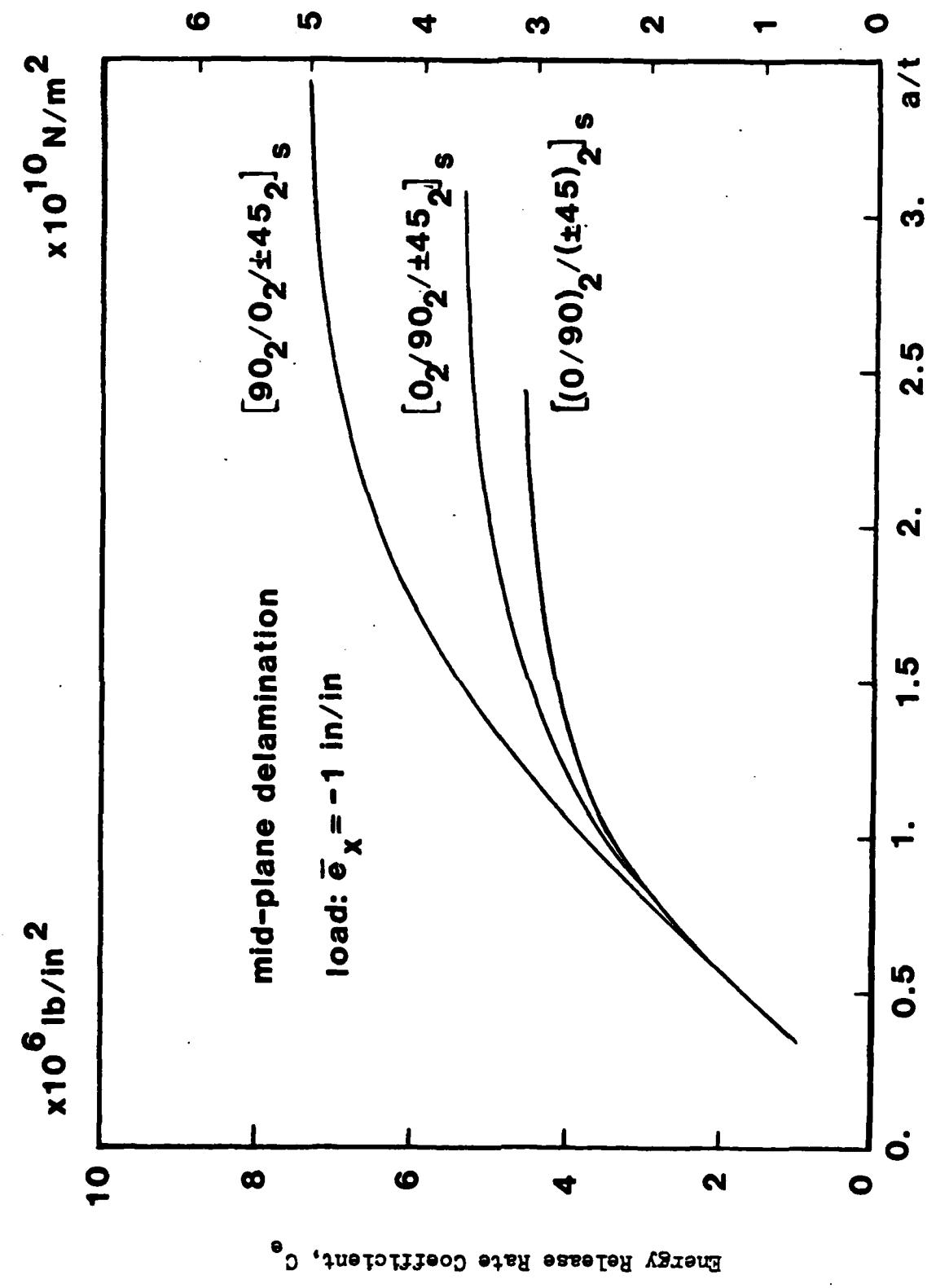

Figure 15. Energy Release Rate Coefficient Function C_e for Delamination Under Compression.

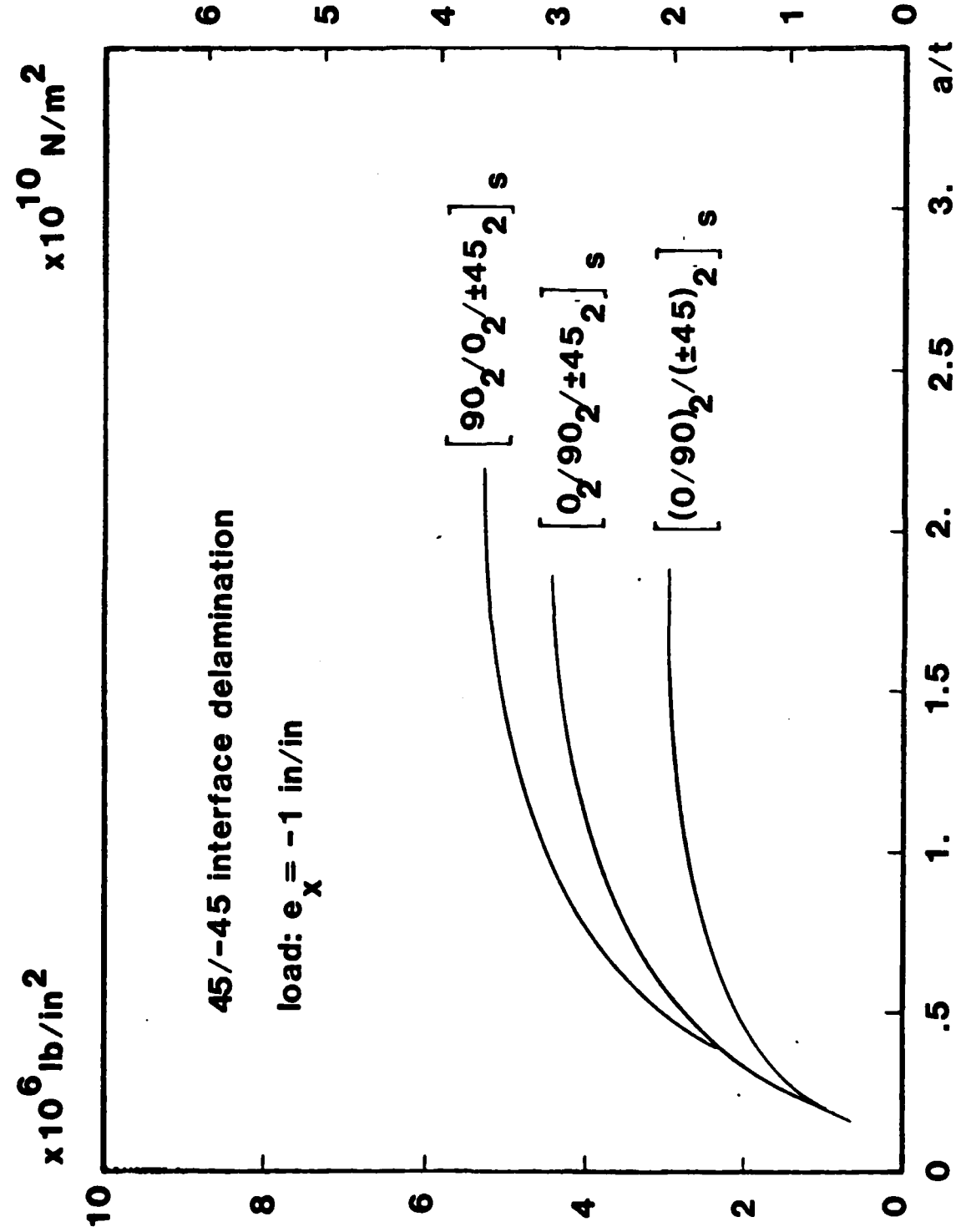

Figure 16. Energy Release Rate Coefficient Function C_e for delamination Under Compression.

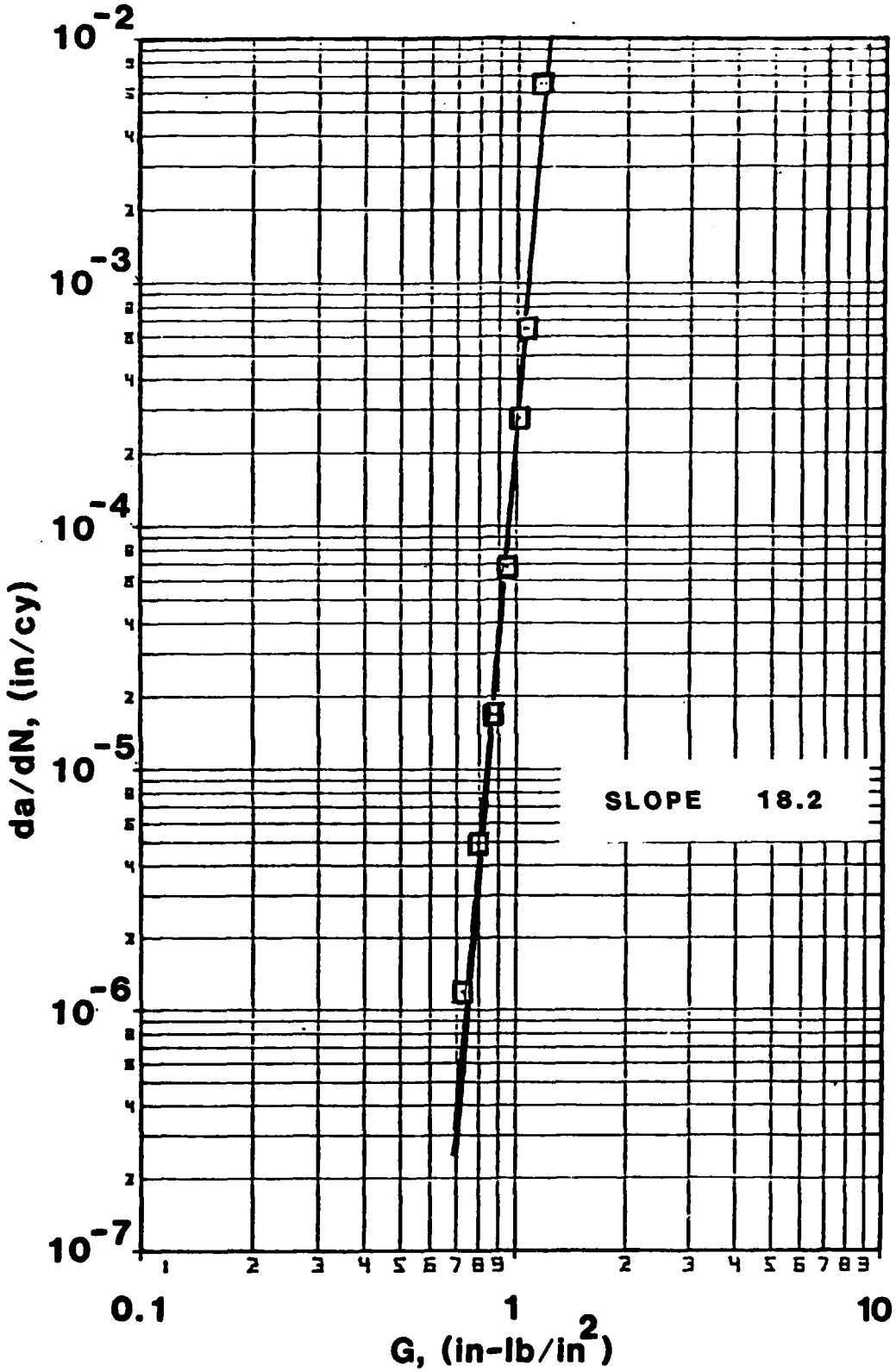

Figure 17. Mode-I Delamination Growth Rate Test. Ref. [23]

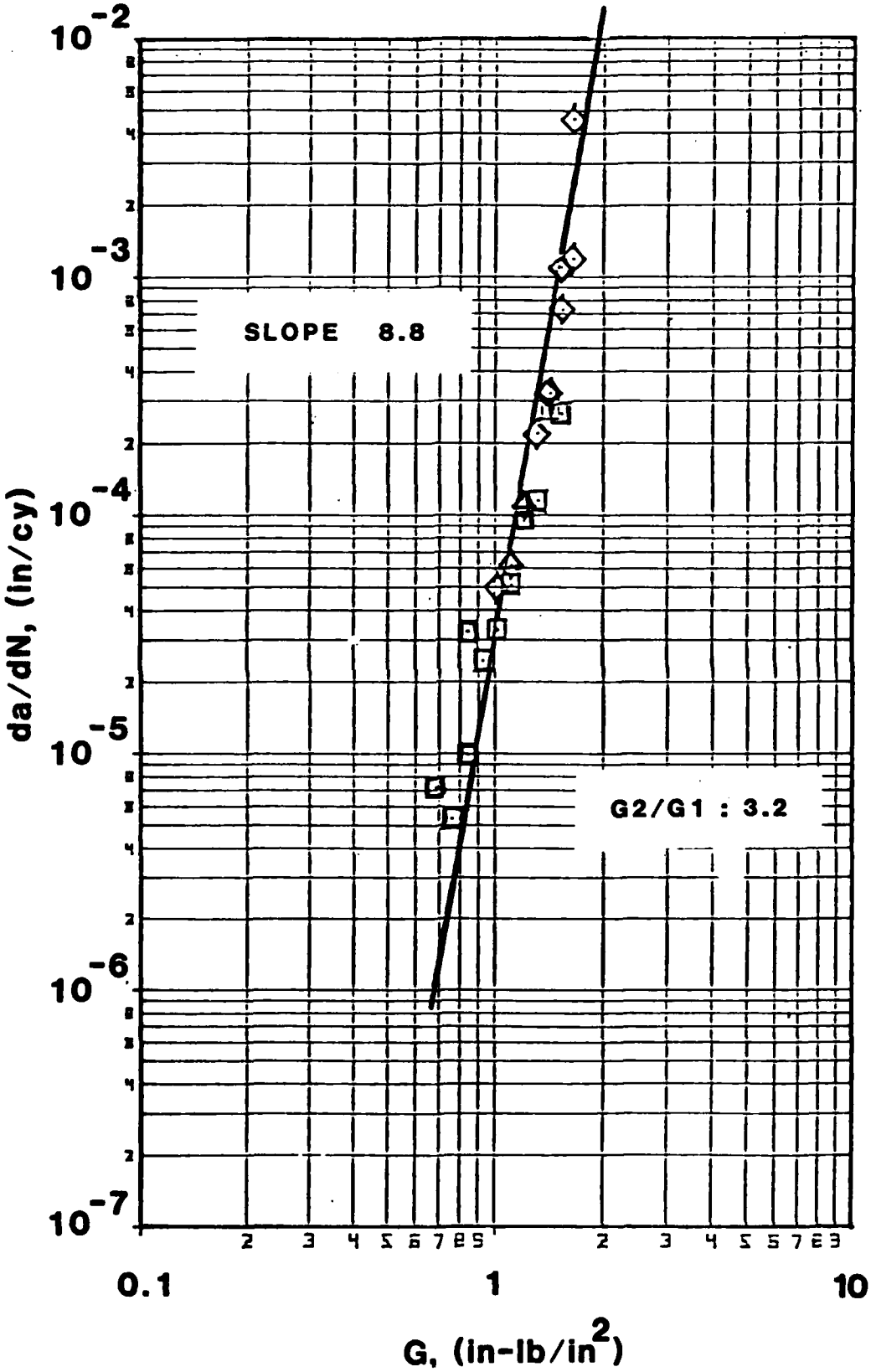

Figure 18. Mixed-Mode Delamination Growth Rate Test. Ref. [23]

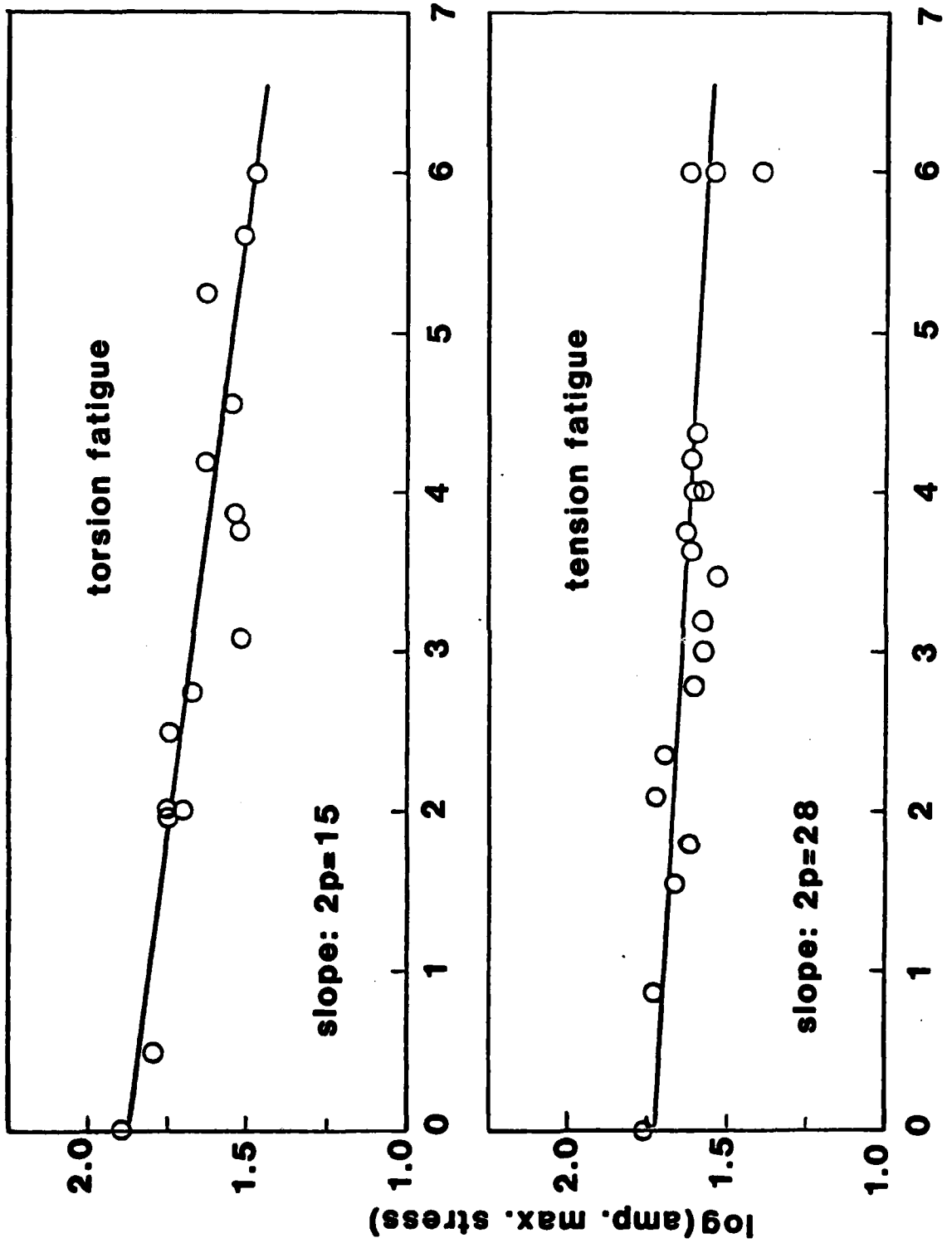

Figure 19. Tension And Torsional Fatigue Test Results of 3501-06 Epoxy Resin. Ref.[32]

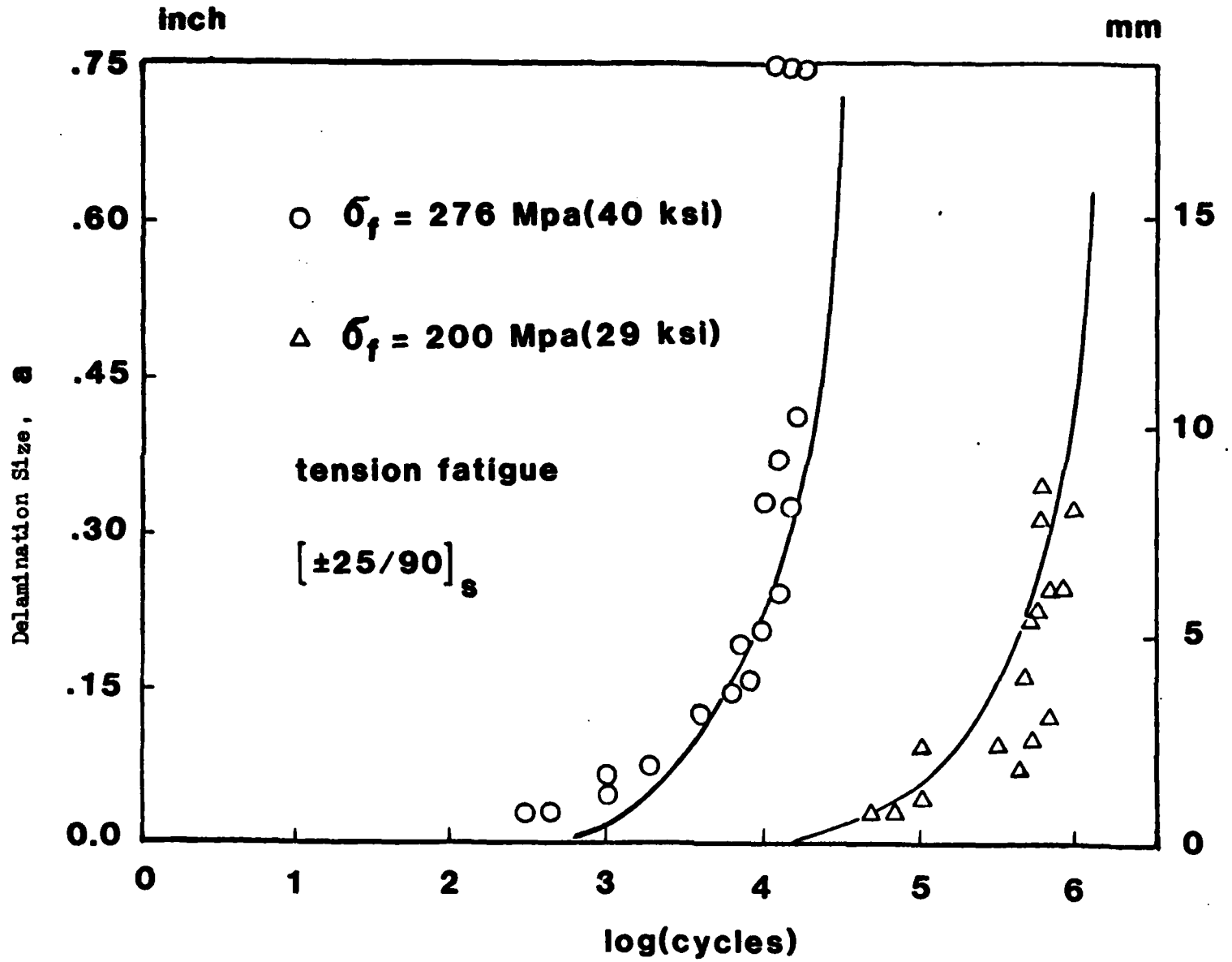

Figure 20. Experiment and Predicted Edge Delamination Growth Under Tension Fatigue. Ref. [30]

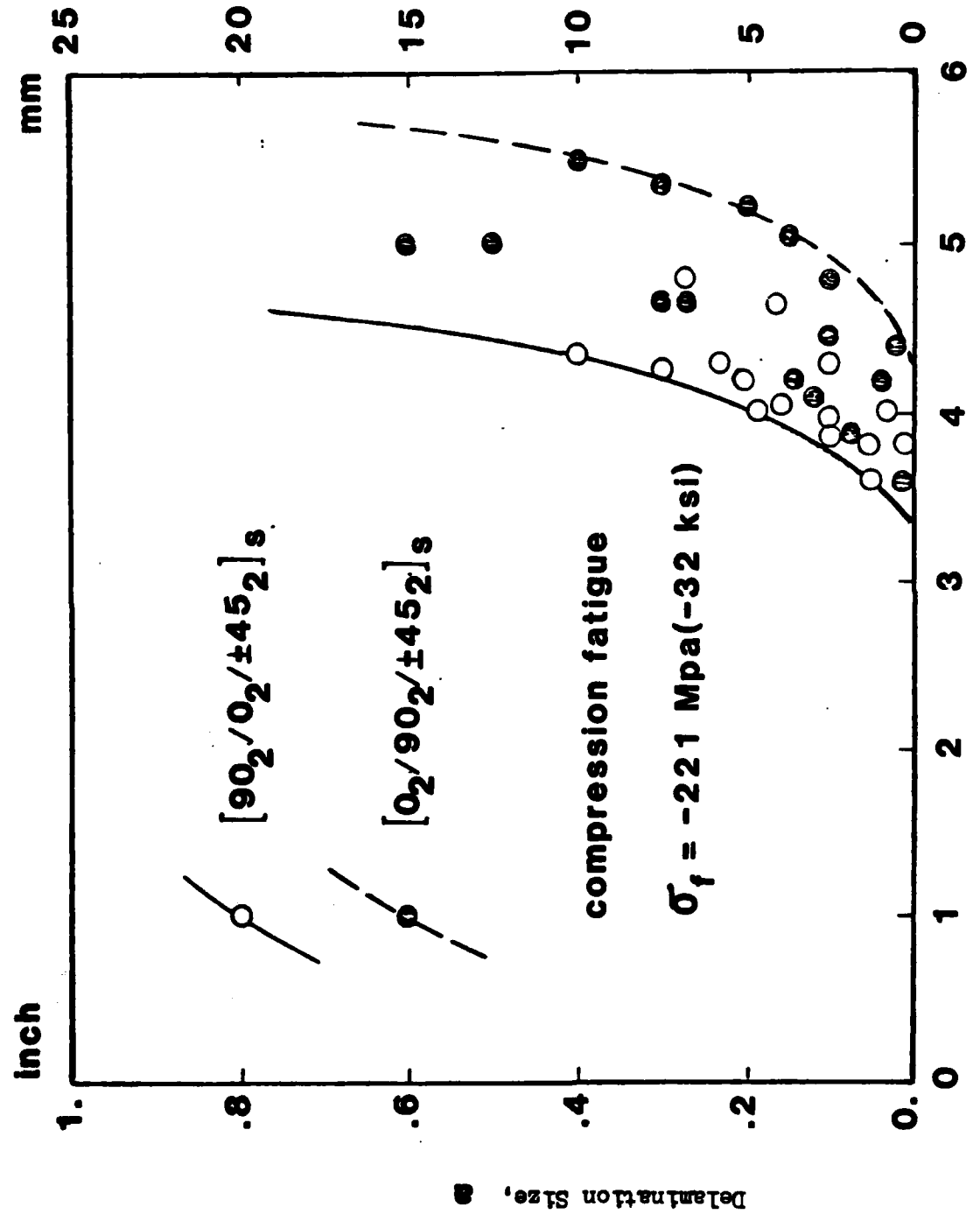

Figure 21. Comparison Between the Experimental and the Predicted Delamination Growth Results

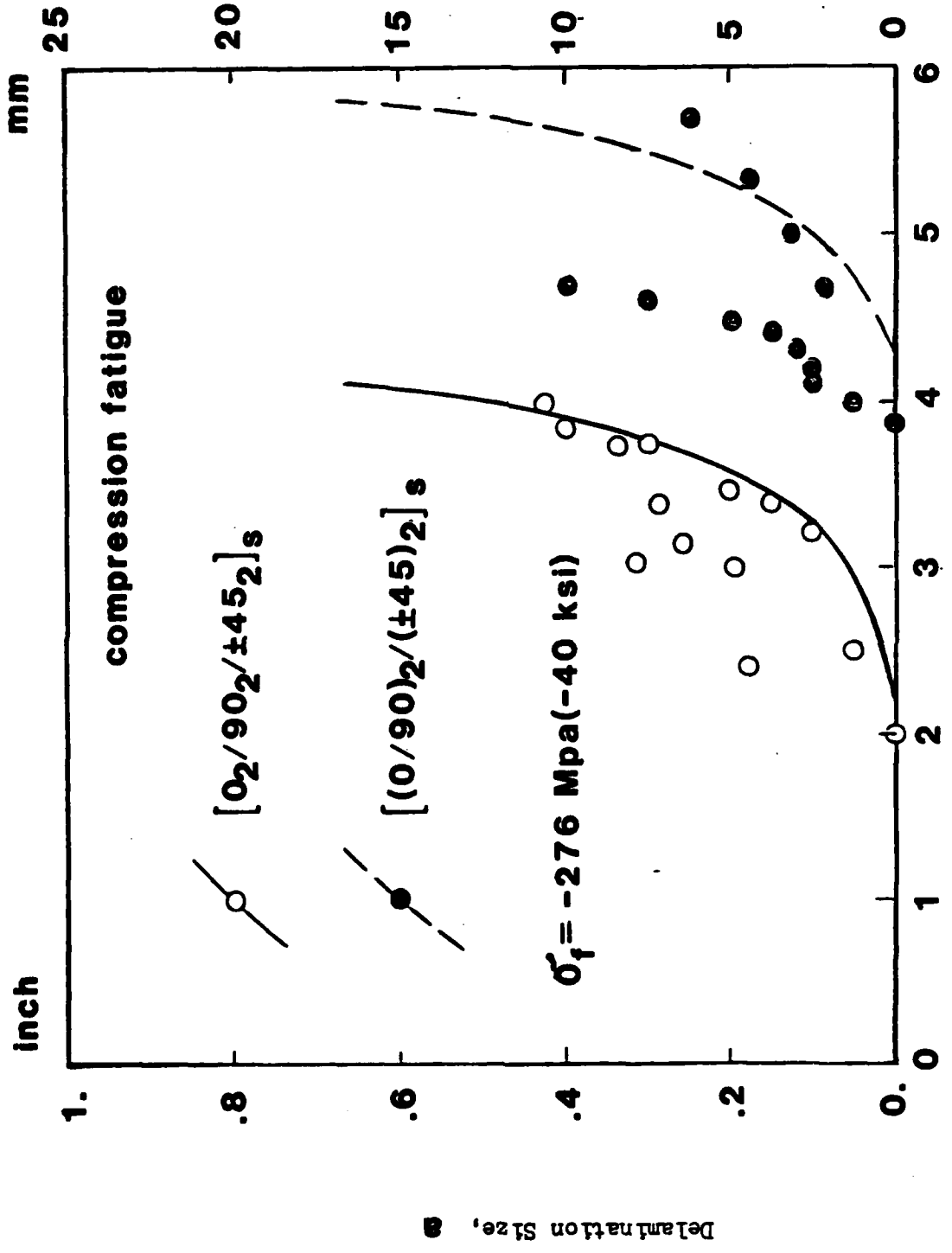

Figure 22. Comparison Between the Experimental and the Predicted Delamination Growth Results.

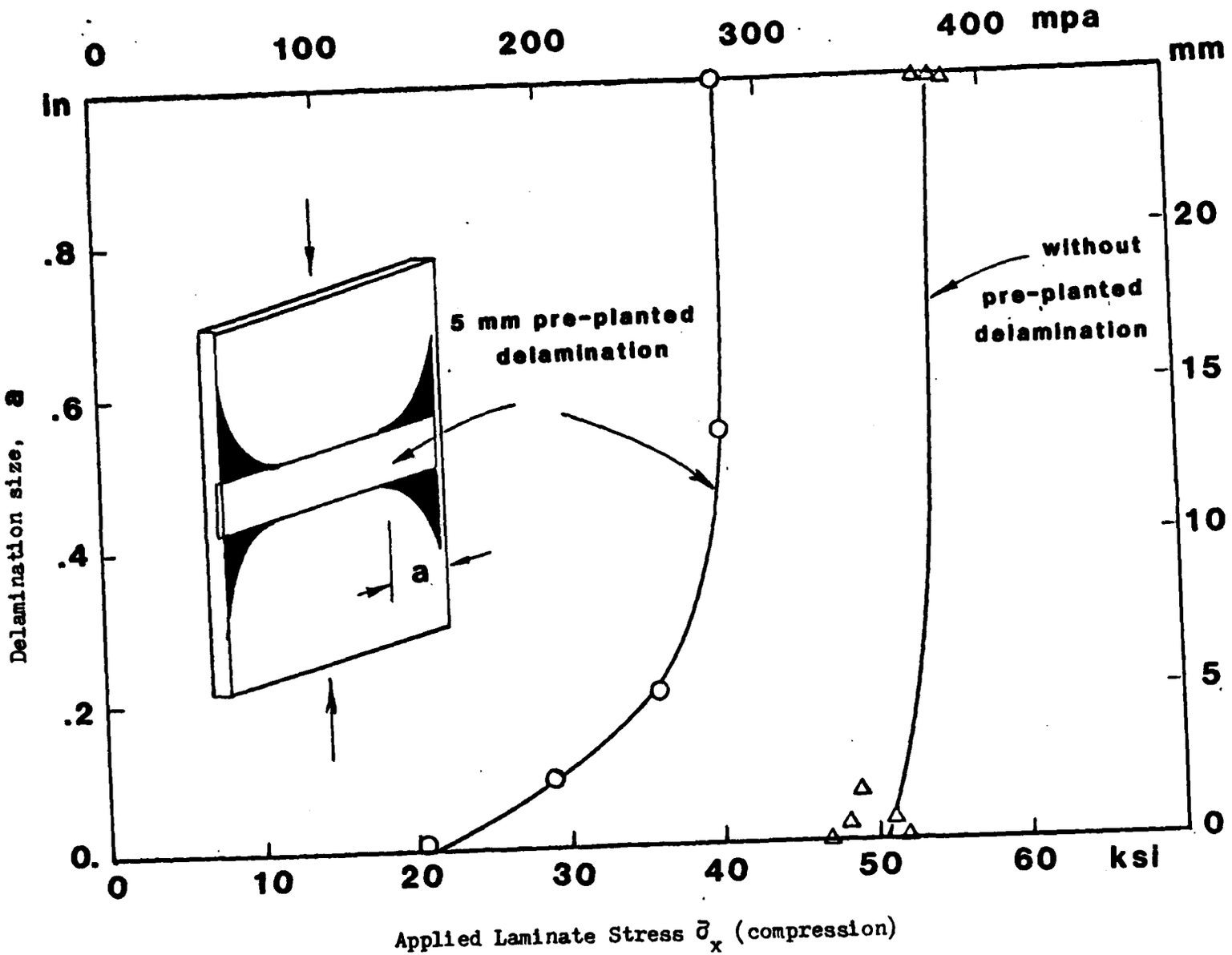

Figure 23. Experimental Delamination Growth In $[0_2/90_2/\pm 45_2]_s$ With and Without Pre-planted Delamination. Ref.[3].

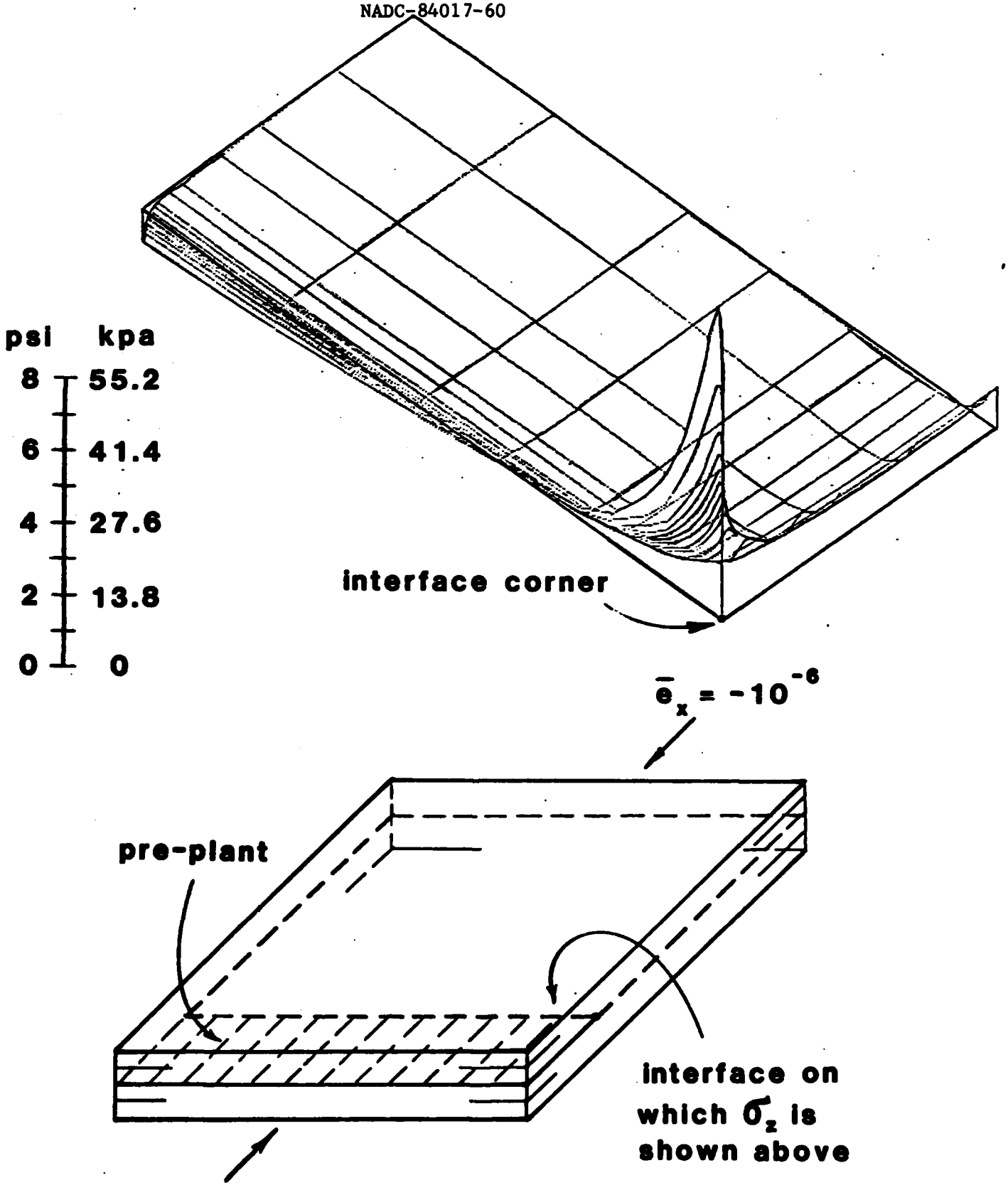

Figure 24. Computed Interlaminar Stress Distribution on Laminate Interface.

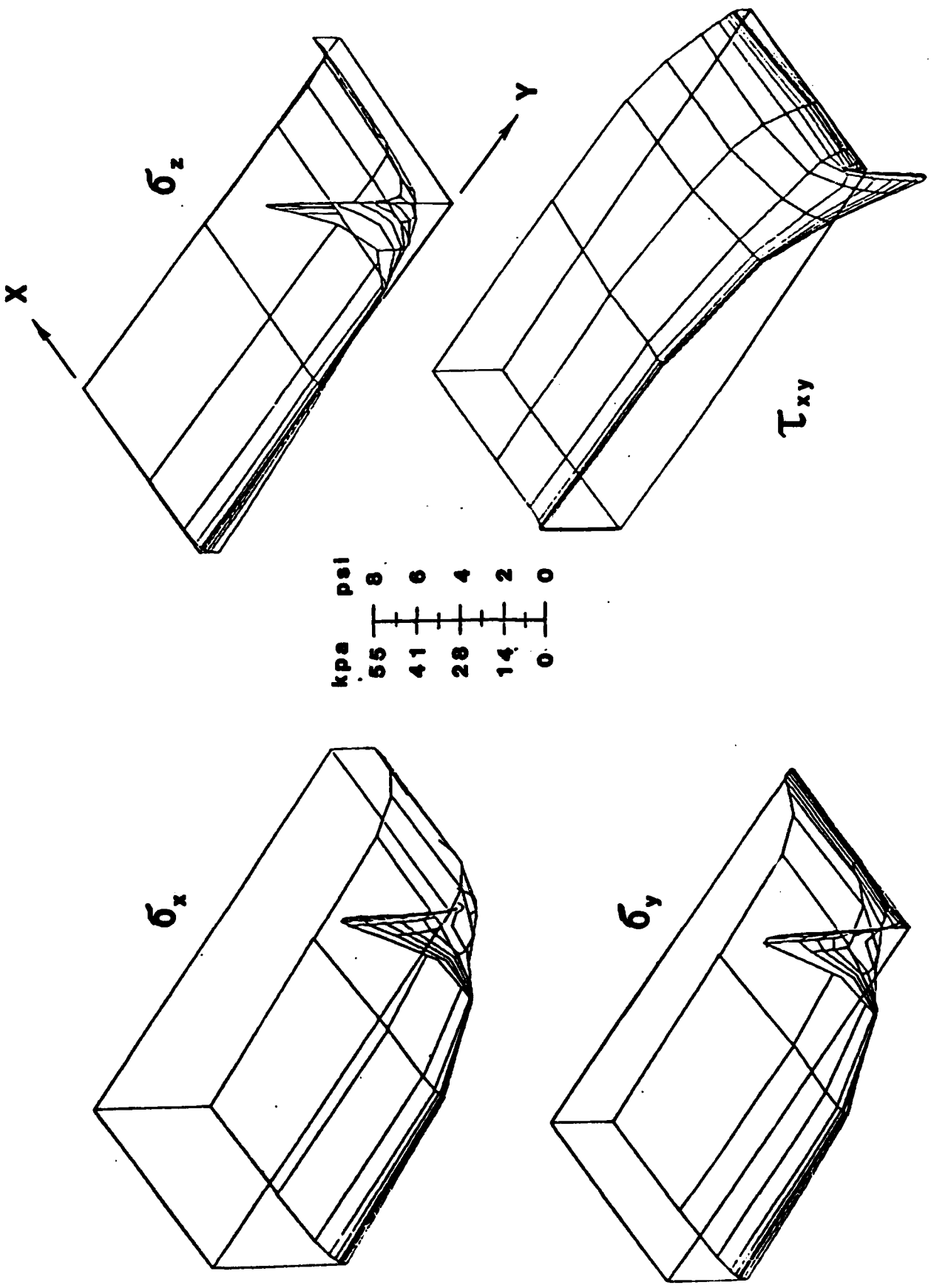

Figure 25. Stresses(non-trivial) in the 45° Layer Immediately Above the Laminate Mid-plane

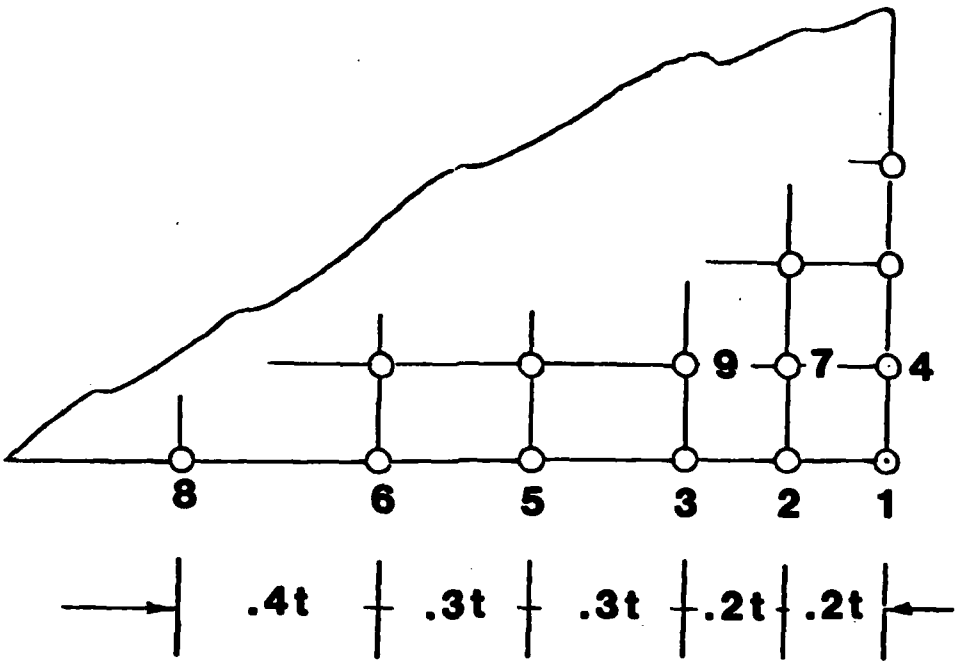

(a)

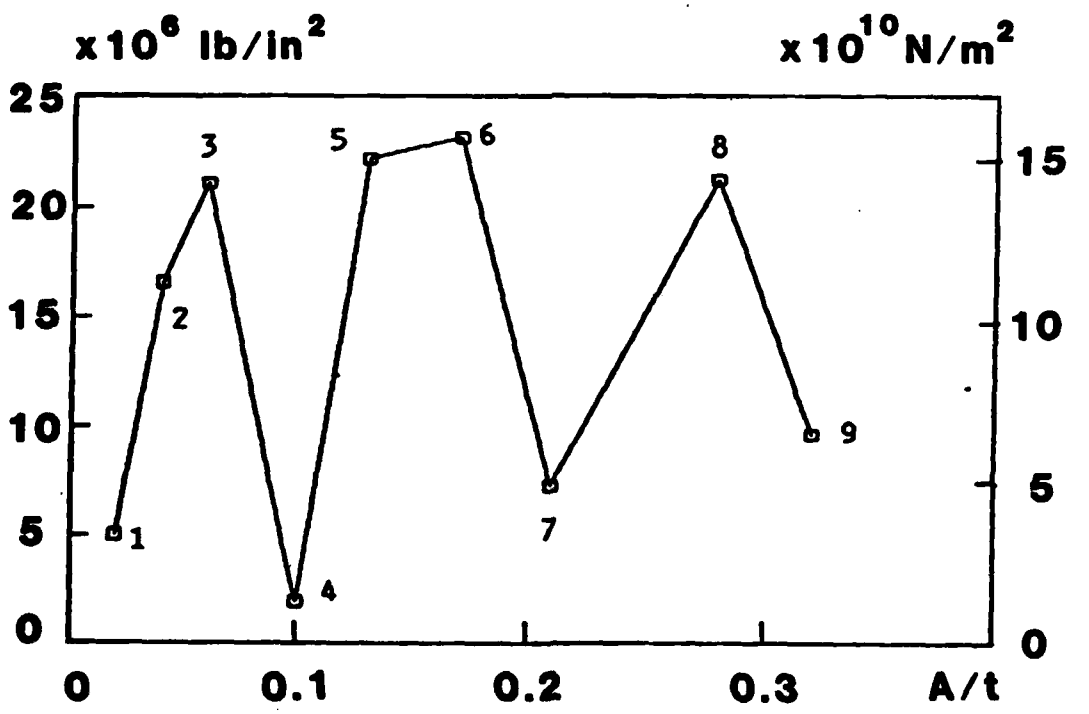

(b)

Figure 26. (a) Nodal Release Sequence Near Interface Corner; (b) Computed C_e Coefficient According to Prescribed Nodal Release Sequence.

Non-Government Agencies (continued)

	No. of Copies
University of Wyoming, Laramie, WY 82071 (Attn: Dr. D. Adams).	1
Villanova University, Villanova, PA 19085 (Attn: Dr. P. V. McLaughlin)	1
Virginia Polytechnic Institute, Blacksburg, VA 24061 (Attn: Dr. K. Reifsnider).	1
Vought Corporation, Dallas, TX 75265 (Attn: Mr. O. E. Dhonau/2-53442)	1
(Attn: Dr. J. Renton).	1

Non-Government Agencies (continued)

	No. of Copies
McDonnell Douglas Corporation, St. Louis, MO 63166	
(Attn: Mr. J. Schier)	1
(Attn: Mr. C. Stenberg)	1
(Attn: Mr. R. Garrett)	1
McDonnell Douglas Corporation, Long Beach, CA 90846	
(Attn: G. Lehman)	1
(Attn: D. Smillie)	1
Minnesota Mining and Manufacturing Company, St. Paul, MN 55104	
(Attn: Mr. W. Davis)	1
Northrop Aircraft Corporation, One Northrop Avenue, Hawthorne, CA 90250	
(Attn: Mr. L. Jeans)	1
(Attn: Mr. D. Stansbarger)	1
(Attn: Mr. R.M. Verette)	1
(Attn: Mr. B. Butler)	1
Owens Corning Fiberglass, Granville, OH 43023	
(Attn: Mr. D. Mettes)	1
Prototype Development Associates, Inc., 1560 Brookhollow Drive, Santa Ana, CA 92705 (Attn: E. L. Stanton)	1
Rockwell International, Columbus, OH 43216	
(Attn: Mr. F. Kaufman)	1
(Attn: Mr. M. Schweiger)	1
Rockwell International, Los Angeles, CA 90009	
(Attn: Dr. Lackman)	1
Rockwell International, Tulsa, OK 74151	
(Attn: Mr. E. Sanders)	1
(Attn: Mr. J. H. Powell)	1
Rohr Corporation, Riverside, CA 92503	
(Attn: Dr. F. Riel)	1
(Attn: Mr. R. Elkin)	1
School of Engineering and Applied Science, Materials Research Laboratory, Washington University, Campus Box 1087, St. Louis, MO 63130 (Attn: T. Hahn)	1
Sikorsky Aircraft, Stratford, CT 06622	
(Attn: Mr. J. Ray)	1
Teledyne Ryan Aeronautical Company, San Diego, CA 92138	
(Attn: Mr. R. Long)	1
Union Carbide Corporation, Cleveland, OH 44101	
(Attn: Dr. H. F. Volk)	1
University of Dayton Research Institute, 300 College Park Ave., Dayton, OH 45469 (Attn: Dr. J. Gallagher)	1
University of Delaware, Mechanics & Aerospace Eng. Dept., Evans Hall, Newark, DE 19711 (Attn: Dr. R. B. Pipes)	1
University of Oklahoma, Norman, OK 73019	
(Attn: Dr. C. W. Bert, School of AMNE)	1

Non-Government Agencies (continued)

	No. of Copies
E. I. DuPont Company, Wilmington, DE 19898 (Attn: Dr. J. Pigoiacampi)	1
Fairchild Republic Company, Farmingdale, L. I., NY 11735 (Attn: Mr. Frank Costa)	1
Georgia Institute of Technology, Atlanta, GA (Attn: Prof. W. H. Horton)	1
General Dynamics/Convair, San Diego, CA 92138 (Attn: Mr. D. R. Dunbar)	1
(Attn: Mr. W. G. Scheck)	1
General Dynamics, Fort Worth, TX 76101 (Attn: Mr. J. A. Fant)	1
(Attn: Dr. D. Wilkins (Composite Structures Eng. Dept.)	1
General Electric Company, Phila., PA 19101 (Attn: Dr. C. Zweben)	1
(Attn: Mr. A. Garber)	1
Great Lakes Carbon Corporation, NY, New York 10017 (Attn: Mr. W. R. Benn, Mgr., Market Development)	1
Grumman Aerospace Corporation, South Oyster Bay Rd., Bethpage, Long Island, NY 11714 (Attn: Mr. R. Hadcock)	1
(Attn: Mr. S. Dastin)	1
Hercules Aerospace Division, P. O. Box 210, Cumberland, MD 21502 (Attn: Mr. D. Hug)	1
HITCO, 1600 West-135th Street, Gardena, CA 90249 (Attn: Mr. N. Myers)	1
ITT Research Institute, Chicago, IL 60616 (Attn: Mr. K. Hofar)	1
J. P. Stevens & Co., Inc., New York, NY 10036 (Attn: Mr. H. I. Shulock)	1
Kaman Aircraft Corporation, Bloomfield, CT 06002 (Attn: Technical Library)	1
Lehigh University, Bethlehem, PA 18015 (Attn: Dr. G. C. Sih)	1
Lockheed-California Co., Burbank, CA 91520 (Attn: Mr. E. K. Walker)	1
(Attn: Mr. Vaughn)	1
(Attn: Mr. A. James)	1
Lockheed-California Co., Rye Canyon Research Lab, Burbank, CA 91520 (Attn: Mr. Don E. Pettit)	1
Lockheed-Georgia Company, Marietta, GA 30063 (Attn: Technical Information Dept., Dept. 72-34, Zone 26)	1
Materials Sciences Corporation, Spring House, PA 19477	1
Philadelphia College of Textiles and Science, School House Lane and Henry Ave., Philadelphia, PA 19144 (Attn: Dr. Frank Ko)	1

DISTRIBUTION LIST

Government Activities

	No. of Copies
NAVAIRSYSCOM, (AIR-00D4), 2 for retention, 2 for AIR-530, 1 for AIR-320B, AIR-52032D, AIR-5302, AIR-53021, AIR-530215)	9
AFWAL, WPAFB, OH 45433	
(Attn: FIBEC, Dr. George Sendeckyj)	1
(Attn: FIB/Mr. L. Kelly, Mr. W. Goesch)	2
(Attn: FIBCA/Mr. C. D. Wallace)	1
(Attn: MLBC/W. B. Jones)	1
(Attn: FIBE/Mr. D. Smith)	1
(Attn: MLBM/Dr. J. Whitney)	1
(Attn: MLB/Mr. Frank Cherry)	1
(Attn: MBC/Reinhart)	1
(Attn: AFWAL/MLSE-Fecheck)	1
Applied Technology Laboratory, USARTL (AVRADCOM) Ft. Eustis, VA 23604 (Attn: Mr. A. J. Gustafson, DAVDL-ATL-ATS, Mr. T. Mazza)	2
Department of the Air Force, Bldg. 410, Bolling Air Force Base, Washington, D.C. 20332 (Attn: Dr. M. Salkind)	1
DTIC	12
FAA, Washington, D.C. 20591 (Attn: J. R. Soderquist)	1
FAA, Technical Center, Atlantic City, N.J. 08405 (Attn: Mr. D. W. Nesterok/Code ACT 330)	1
NASA, Washington, D.C. 20546 (Attn: Mr. Charles Bersh)	1
NASA, George C. Marshall Space Flight Center, Huntsville, AL 35812 (Attn: S&E-ASTN-ES/Mr. E. E. Engler)	1
(Attn: S&E-ASTN-M/Mr. R. Schwinghamer)	1
NASA, Langley Research Center, Hampton, VA 23665 (Attn: Dr. J. R. Davidson, M.S. 188E; Dr. J. Starnes, M.S. 190; Dr. J. Williams, M.S. 190, Dr. M. Mikulus, Mr. H. Bohan, and Dr. C. P. Blakenship; M.S. 188M)	6
NASA, Lewis Research Center, Cleveland, OH 44135 (Attn: Dr. C. Chamis, M.S. 49-6 and M. Hershberg)	2
NAVAIRDEVCEN, Warminster, PA 18974 (Attn: Major J. Keane - 097); 3 for Code 8131)	4
NAVPGSCOL, Monterey, CA 95940 (Attn: Prof. R. Ball, Prof. M. H. Bank)	2
NAVSEASYSCOM, Crystal Mall 4, Rm. 109, Washington, D.C. 20360 (Attn: Dr. H. Vanderveldt)	1
NAVSEC, Arlington, VA 20360 (Attn: NSEC-6101E)	1
NAVSHIPRANDCEN, Bethesda, MD 20084 (Attn: Code 173.2, Mr. W. P. Couch)	1
NAVSHIPRANDCEN, Annapolis, MD 21402 (Attn: Code 2870, Mr. H. Edelstein)	1
NAVAL SURFACE WEAPONS CENTER, White Oak Laboratory, Silver Spring, MD 20910 (Attn: Dr. J. Goff, Materials Evaluation Branch (R-34)	1

Government Activities (continued)

	No. of Copies
NOL, White Oak, MD 20910 (Attn: Mr. F. R. Barnet)	1
NRL, Washington, D.C. 20375 (Attn: Dr. I. Wolock)	1
ONR, Washington, D.C. 20362 (Attn: Dr. N. Perrone)	1
PLASTEC, Picatinny Arsenal, Dover, NJ 07801 (Attn: Mr. H. Pebly)	1
(Attn: Librarian, Code DRDAR-SCM-O, Bldg. 351-N	1
U. S. Army Materials and Mechanics Research Center (DRXMR-PL) Watertown, MA 02172 (Attn: Dr. E. Lenoe)	1
(Attn: Mr. D. Oplinger)	1
U. S. Army Research Office, Durham, NC 27701	1
U. S. Army R&T Lab (AVRADCOM), Ames Research Center, Moffett Field, CA 94035 (Attn: Mr. F. Immen, DAVDL-AS-M.S. 207-5, Dr. R. Foye)	2
David Taylor Naval Ship Research & Development Center, Code 2822, Annapolis, MD 21402 (Attn: Mr. A. Macander, Mr. R. Crane)	2

Non-Government Activities

Avco, Aero Structures Division, Nashville, TN 37210	1
Battelle Columbus Laboratories, Metals and Ceramics Information Center, 505 King Avenue, Columbus, OH 43201	1
Bell Aerospace Company, Buffalo, NY 14240 (Attn: Zone I-85, Mr. F. M. Anthony)	1
Bell Helicopter Company, Fort Worth, TX 76101 (Attn: Mr. G. Reis Alsmiller, Jr.)	1
Bendix Products Aerospace Division, South Bend, IN 46619 (Attn: Mr. R. V. Cervelli)	1
Boeing Company, P. O. Box 3707, Seattle, WA 98124 (Attn: Mr. R. E. Horton, MS 9K-23)	1
(Attn: Dr. R. June)	1
Boeing Company, Vertol Division, P. O. Box 16858, Philadelphia, PA 19142 (Attn: Mr. R. L. Pinckney)	1
(Attn: Mr. D. Hoffstedt)	1
(Attn: Mr. L. Marchinski)	1
Boeing Company, Wichita, KS 67210 (Attn: R. D. Hoaglanb - M. S. -K32-95)	1
Cabot Corporation, Billerica Research Center, Billerica, MA 01821	1
Drexel University, Phila., PA 19104 (Attn: Dr. P.C. Chou)	1
(Attn: Dr. A.S.D. Wang)	1

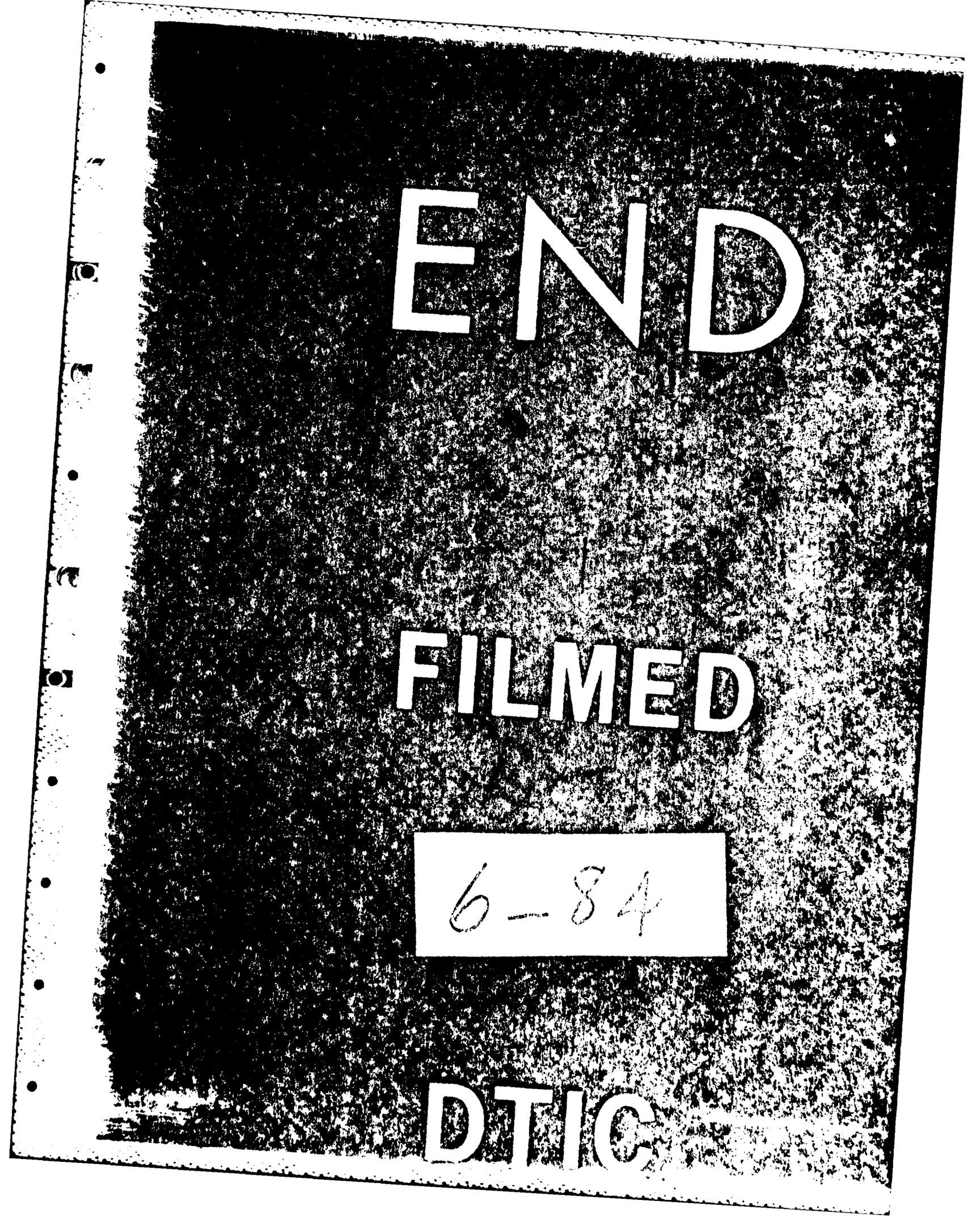
END
FILMED
6-84
DTIC